NASA Contractor Report 3658

Determination of Physical and Chemical States of Lubricants in Concentrated Contacts - Part 3

James L. Lauer and Leonhard Keller

GRANT NSG-3170
JANUARY 1983

NASA

NASA Contractor Report 3658

Determination of Physical and Chemical States of Lubricants in Concentrated Contacts - Part 3

James L. Lauer and Leonhard Keller
Rensselaer Polytechnic Institute
Troy, New York

Prepared for
Lewis Research Center
under Grant NSG-3170

National Aeronautics
and Space Administration

**Scientific and Technical
Information Branch**

1983

TABLE OF CONTENTS

PART 1

INTRODUCTION

Why do bearings fail? Machinery may run quietly for a long time and then suddenly the bearing may become noisy or seize. Examination will then show scoring of the surfaces and the lubricant will be contaminated. This catastropic failure phenomenon is generally called scuffing although experts differ in their terminology. Although much work has been done on scuffing, the basics are still not understood: What fails first, the lubricant or the surfaces? Is pressure, temperture or speed the determining factor? How is the chemistry of the bearing system involved.

Most experts agree that scuffing requires a high flash temperature. By this they mean a sudden increase in temperature produced by direct metal-to-metal contact. The lubricant should minimize such contacts. The selection of the lubricant is usually made primarily on the basis of viscosity as measured under ambient conditions. One reason for the work of this report was to determine the changes of viscosity of lubricant additive packages under operating conditions. The procedure involved primarily infrared emission spectrophotometry of an operating mock bearing. Infrared spectroscopy is a powerful technique which is sensitive to the thermal motions within molecular and crystal entities. In fact, it determines the mechanical modes of vibration of the atoms. These modes portray the structure and alignment of the molecules. Resonances with polarized infrared radiation are indicative of preferred molecular directions.

In this work, molecular alignment of the lubricant in a bearing contact was found to vary with shear rate in a rather direct

way, so that the alignment is almost certainly caused by fluid flow and not, for example, by adsorption on bearing surfaces. Molecular alignment is associated with a lowering of viscosity. The additive studied--or contaminant--1,1,2-trichloroethane increased the alignment even when present in small concentration. The reason for this behavior could be adsorption on the surfaces or a bulk effect. Substitution of the steel ball surfaces by a titanium-nitride surface and other tests on the fluid showed that both a bulk and a surface effect were playing a role. Furthermore, no scuffing was ever observed with titanium nitride-coated surfaces--a very definite and concrete result of this study.

The infrared analysis of the very thin films (typically about 1000Å thick) of lubricants is not essentially different from the analysis of deposits on aircraft fuel lines. There the problem is not scuffing but reduction of heat transfer as deposits are formed. The most interesting result was the effect of rapid oxidation of deposits already formed--apparently the polymerized material became more amorphous and therefore more tacky.

For all this work significantly new apparatus had to be designed and built. Changes of existing computer program packages were also made. This work, which will be discussed in some detail in the body of this report, already resulted in three publications [11], [12], [13] and three presentations at technical society meetings.

Mr. Frank H. Choi provided the data on traction and film thickness; Mr. Peter Frauenknecht assisted with the computer programs; and Mr. James Kloiber constructed the thermostatted circulation system.

Mr. James Szappanos and Dr. David Kaneshiro of Janos Optical Company in Townstend, Vermont worked with us trying to solve the beamsplitter problems. Mr. Braedle of SKF-Switzerland donated the bearing balls which Drs. Hinterman and Boving of Laboratoire Suisse coated for us with titanium nitride. Dr. E.G. Brame and Mr. A. Boyd of the duPont Company made an R11C-FS-720 Fourier spectrophotometer available to us.

This work was also supported by a grant from the Air Force Office of Scientific Research (AFOSR-78-3473).

PART 2

BACKGROUND

The practical problems that gave the impetus to the study of scuffing in a simulated ball bearing by infrared emission Fourier microspectrophotometry was the frequent failure of helicopter transmissions soon after an overhaul. The problems were assumed to be due to the cleaning of the parts with organic chlorides prior to an overhaul. The work was started in the early 70's at Sun Oil Company at Marcus Hook, Pa, [14], [15] and later continued by V.W. King [2] under the supervision of Dr. J.L. Lauer at R.P.I., Troy, N.Y. This report is the temporary conclusion of this work.

The geometry of a simulated ball bearing, i.e. a bearing ball sliding on a plate, allows only one window in the contact. Since the transmission of infrared radiation is not possible in this arrangement, reflective techniques would be required for the operation of an absorption instrument. Because of the small size of the area of interest, (the Hertzian area) and the ease of use, emission spectroscopy was chosen.

Low and Coleman [16] recognized that the energy limitations imposed by just moderately heated sources can be overcome by Fourier interferometry. With the significantly larger signal to noise ratio of a Fourier emission interferometer over a dispersion instrument at comparable speed and resolution they were able to measure the spectra of silicone grease, oleic acid and other materials

deposited on aluminium and heated to about 40°C (detector at ambient). A quantitative comparison of these two types of interferometer is given in Part 3.

In his doctoral thesis [2] V.W. King found besides a temperature gradient, oriented molecules of the lubricant in a simulated EHD (Elasto-Hydrodynamic) ball/plate contact. For the continuation of the studies he recommended the introduction of a rotating polarizer--a device taking optically the spectral difference of two directions perpendicular to each other and therefore eliminating the randomly oriented background--as a desirable increase in spectral contrast (baseline emission bandstrength to background ratio). Since the operation of the installed blackbody temperature reference and the alignment of the instrument itself--a FS720 RIIC Beckman absorption instrument converted to an emission instrument--required a lot of skill and luck, it was decided to build a new and easily alignable emission module for the basic commercial instrument. The new module comprises the mechanics for a rotating polarizer, a blackbody reference adjustable in temperature and flux, a mirror holder and a chopper. For a further increase in resolution and sensitivity, provision for the attachment of a new microscope lens with higher magnification (36X instead of 15X) and a larger numerical aperture (.50 instead of .28) had to be made.

During initial testing it became obvious that with the improved spectral contrast, sensitivity and resolution, the instrument is well suited for the analysis of deposits adsorbed on metallic surfaces, which

are often polarized because of preferred directions during deposition. Besides the studies of lubricants in an EHD contact, work was done analyzing static samples, i.e. deposits on aircraft fuel lines. The common instrument for both studies explains why two apparently different subjects are treated in this report, namely the alignment of fluid molecules in an EHD contact and the analysis of aircraft fuel line deposits.

2.1 Physical and Chemical Problems of an EHD Contact

The state of the lubricant in an EHD contact is still largely unknown. Is the lubricant a liquid or a glass or a composite? What is the special property of torque-transmitting (traction) fluids? Winer et al. [7] modeled them as glasses of relatively high yield stress in the Hertzian contact region. Winer calculated the observed traction coefficients from them--a remarkable achievement. However, he did not attempt to correlate the chemical structure and physical properties of these fluids with their behavior in concentrated contacts. An almost linear relationship has been shown between traction coefficient and traction fluid concentration for traction/ester lubricant solutions. On the other hand, sharp decreases of traction occur for small concentrations of some additives such as organic chlorides. A large effect of small concentrations of additives would require a mechanism by which these additives are concentrated in the contact region, such as adsorption on the bounding surfaces. On the other hand, effects proportional to concentration would seem to be bulk effects. Polyphenyl ether also has torque-transmitting properties and has been studied by many investigators because of its

very high temperature stability. This fluid has been described as viscoelastic, plastic, or glassy.

The behavior of boundary additives in lubricants has been generally accounted for by surface adsorption in the Hardy and Bowden-Tabor theories. Similar adsorptive behavior would be expected to prevail under EHD lubrication as well. However, Okabe and Kanno [18] showed that the adsorption theories for boundary lubrication were oversimplified, for wear prevention continued to improve for solutions of squalane containing polar additives as the concentrations were increased well beyond those required for the formation of monomolecular layers. Furthermore, wear prevention did not correspond to measures of the adsorptivity of the polar groups so that a mysterious "structural property" acquired by the bulk lubricant was invoked. The modifications described by Rounds [19] of the susceptibility toward additives which was found to result from the presence of certain other additives in particular fluids are another example of the failure of accounting for concentrations of minor constituents in contacts solely by adsorption on the metal surfaces.

While the emission microspectrophotometer is sensitive enough for the general analysis of EHD contact regions, it can not be used to analyze a few molecular layers of lubricant additives on surfaces in the presence of bulk fluid. Even the addition of the differential polarization adapter proved inadequate for this task. Yet, the spectral comparison of the influence of a metallic (440C Stainless Steel) with a chemically inert (TiN) ball surface, but identical bulk properties, on the fluid together with glass transition and temperature measurements, did help to find a bulk fluid

effect in the contact region. This goes a long way toward explaining the "mysterious structural property" acquired by the bulk fluid as a result of the presence of additives. Namely, the additives help change the orientation of the bulk fluid molecules, which is produced by the high shear rates in EHD contacts. They may do that by initiating separation under the high contact pressures and cause two-phase shear flow in the contact. The hydrodynamics of the situation would also seem capable of providing an additional mechanism to account for an accumulation of additive in the contact region.

This work has led to a new model for EHD and boundary lubrication in the presence of polar additives. This model is also consistent with the observation of drastic reductions of traction coefficients by small concentrations of polar additives.

2.2 Deposits on Aircraft Fuel Lines

Until recently the deposition of carbonaceous fuel residues on fuel lines and other surfaces in operating aircraft was a minor problem, since mid-distillates from petroleum are generally rather clean and thermally stable. In other words, their aromatics, sulfur and nitrogen contents are low, and their volatility relatively high. However, the supply of these mid-distillates has been shrinking so that a relaxation of specifications seems inevitable.

Griffith [20] recognized during his early work on emission spectroscopy, that thick samples--presumably due to a temperature gradient--reduce the spectral contrast drastically. Initially the temperature gradient was hoped to be suppressed by mounting an infrared transparent KCℓ window on top of the sample. Samples with a low conductivity still showed inversions in their spectra and required

further improvement. With a newly designed heating system the sample is heated from two sides by the same temperature source, which also heats the blackbody reference.

Deposit formation was expected to be dependent on temperature gradient. A sample would therefore show different deposits at different locations. Reproducible scanning of a sample was achieved by mounting the sample holder in a precision x,y,z stage with an oversize turntable.

The spectra of a fuel sample are not easily interpreted. The presence of numerous components decreases the spectral contrast and weak bands are lost. The use of the polarizer proved to be helpful, because it allows the detection of weak bands near a strong band, assuming they are differently oriented.

PART 3

THEORY

The origin of infrared emission is treated first. In the second section, a model for the alignment of molecules due to flow and a description of the evaluation of data from oriented material are given. The description of the Michelson interferometer explains how infrared radiation is transformed from the time domain into the frequency domain for the analysis. Finally a short analysis of an EHD contact is given.

3.1 The Nature of Infrared Emission

Infrared radiation is electromagnetic in origin and therefore caused by an oscillating electric field such as the one produced by a change of an electric dipole moment, which is the vector between the centers of positive and negative charge.

3.1.1 Infrared Radiation of Molecules

Using a mechanical model consisting of mass points and springs for a molecule, the modes of vibrations (Figure 3.1) and the normal frequencies can be computed [5]. Assuming differences in electric charges for neighboring mass points--corresponding to the type of binding between atoms (covalent, ionic)--dipole will moments exist. However, emission of infrared radiation will only take place, if the vibrations produce an alternating electric field; i.e. if the vibrations are coupled with a changing dipole moment. The frequency of the radiation is identical to the frequency of the oscillating dipole. In general, the fundamentals of molecular

Linear Molecule

symmetric stretching vibration

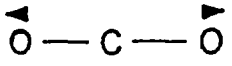

asymmetric stretching vibration

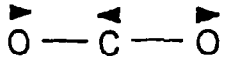

bending vibration

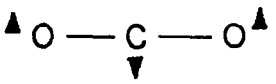

Bent Triatomic Molecule

symmetric stretching mode

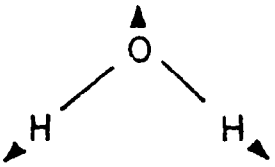

asymmetric stretching mode

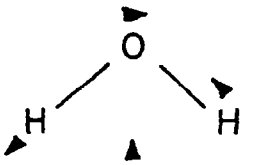

symmetric bending mode

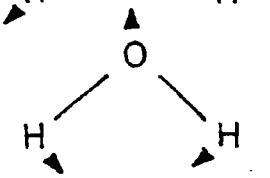

Figure 3.1 Modes of vibration of CO_2 and H_2O

vibrations fall between 4000 cm^{-1}* and 400 cm^{-1}, the principal infrared region.

Since many molecules in the liquid or solid phase will always be observed, where the interaction between molecules plays an important role, the emission of rotational energy is not important. Depending on the environment interaction between molecules varies strongly. In extreme cases shifts of the normal frequencies occur.

Absorption of infrared radiation will occur if the frequency of the radiation is identical to the natural frequency of the molecule. In thermal equilibrium, a molecule absorbs and emits the same amount of energy. Therefore, radiation is absorbed if radiation of a hot continuum source, e.g. graybody, is passed through a dielectric material. On the other hand, radiation is emitted if the surroundings, e.g. the detector, is cooler. However, a non-isothermal film will partially reabsorb emitted radiation within the layer, even in the case of lower surrounding temperature.

3.1.2 Continuum Source or Blackbody Radiation

According to the well known Planck distribution law, the spectral distribution of energy emitted by an ideal blackbody is determined solely by the temperature of the radiating element

---

* Wavenumber: number of waves per cm. It is proportional to the frequency and to the reciprocal of the wavelength measured in vacuum. It is expressed in cm^{-1}.

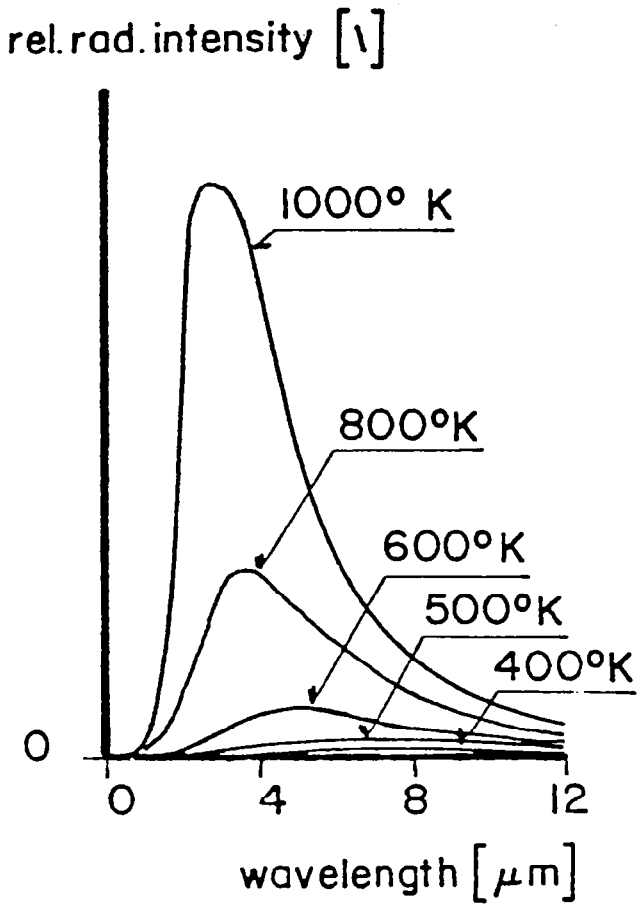

Figure 3.2 The Planck radiation law

(Figure 3.2). Although a true blackbody is a theoretical concept, repeated interaction of electromagnetic radiation, as in a cavity of a metallic material of relatively low emissivity ($\tilde{=}$ .4), will yield "blackbody" radiation with an emissivity of about 0.98 or 0.99 [6].

The maximum of the Planck distribution shifts at higher temperatures to shorter wavelengths. For 300°K the maximum is about 1000 cm^{-1}. This allows measurement of emission spectra of samples slightly above room temperature at the maximum energy in the spectral region of our instrument.

3.2 Molecular Alignment

3.2.1 Flow Orientation of Macromolecules

The alignment of macromolecules by flow is described extensively in the literature [9]. With some restrictions, this theory is adaptable to the size of molecules used in this study. The similarity of the problems led to the presumption, that even relatively small molecules will be oriented by a velocity gradient present in nearly any practical flow.

A short treatment of the "necklace model" [10] to analyze the orientation of a macromolecule by flow is given here. The macromolecule, which is assumed to be suspended in a solvent, is replaced by an appropriate number of Z links with the length A. The extended model has the same length L as the extended macromolecule.

$$L = Z \cdot A \qquad (3.1)$$

The vector $\underline{h}$, which is important for the description of the practical behavior of the macromolecule, is defined by the starting and ending point of the macromolecule. If it can be shown that if the distribution of the vector $\underline{h}$ is a function of the flow, then the problem is solved. For the static situation (no flow), statistical analysis gives the average of the squared value of the $\underline{h}$ vector for a polymer as a function of link length and number of links. It is therfore a circular distribution, independent of angle.

$$\langle h^2 \rangle = ZA^2 \tag{3.2}$$

In this model, the different forces due to a velocity gradient in the solvent are thought of as acting at the end points of the molecule only, instead of forces being distributed continuously over the whole length. Thus the model is reduced to an elastic dumbbell, two spheres at a distance $|\underline{h}|$ apart. The "free" end is subjected to three influences: it is moved by the flow and by a restressing force (spring-like behavior) and pushed by Brownian motion in the direction of steepest descent of the distribution function. Consequently a nonuniform angular distribution or alignment is established depending on the velocity gradient of the flow.

3.2.2 Evaluation of Spectral Data From Oriented Material

The philosophy of using a polarizer for spectral measurement is twofold. The data can be used for the analysis of the projected angular distribution function, which means the orientation of a particular transition moment. Secondly, the polarizer can be used to increase the sensitivity and resolution of the

microspectrophotometer for the measurement of oriented material. The first application applies best to the ball experiment, where the sample is known. The second is applied best to the analysis of an unknown deposit.

Only preliminary work has been done on evaluation of the data. Further analysis appears in Part 5. In the following subsections the analysis of the orientation of a transition moment and a description of the problems of the calculation of orientation are given.

3.2.2.1 Orientation of a particular transition moment. Assume all molecules of a sample to be parallel and oriented in the same direction. The relative intensity I_B of a transition moment in the axis of the molecules plotted against the angle ϕ between the direction of observation and a reference plane, will yield a function of the type,

$$I_b(\sigma) = I_{BG}(\sigma) + I_A(\sigma) \cdot \cos^2(\phi - \nu) \qquad (3.3)$$

where I_{BG} is the relative intensity due to the random background radiation, I_A the relative intensity due to the transition moment in the molecular axis and ν a phase angle given by the orientation of the reference plane. The orientation of the molecule or transition moment is given by $\nu = \phi$. In general the angular distribution function is more complex than assumed in the previous example.

The intensity distribution of a particular transition moment, as a function of the angle ϕ, is equal to the convolution of the angular distribution function in the X,Y, plane with the polarizer line shape function.

A series of spectral measurements with different polarizer settings yields the intensity distribution. The instrument line shape function of the polarizer is of the $\cos^2 \phi$ type. Knowing this function, a deconvolution of the measured intensity distribution is possible. The calculation of the spatial function requires a second set of data ideally recorded in a plane perpendicular to the first one.

Attempts to determine the degree of polarization, like the normalized standard deviation of $I_B(\sigma)$ were not succesful. The method for the calculation of the two dimensional angular distribution function has not been carried out.

3.2.2.2 Proposal of a method for the calculation of molecular orientation. The observation of oriented material will not allow the direction measurements of angles between transition moments. The angle seen is always the projected angle. Since the structure of the molecule is assumed to be known and rigid, the real value of any angle is given. In addition, the interpretation of the phase angle has to be done very carefully because it gives only the orientation, but not the direction of the transition moment.

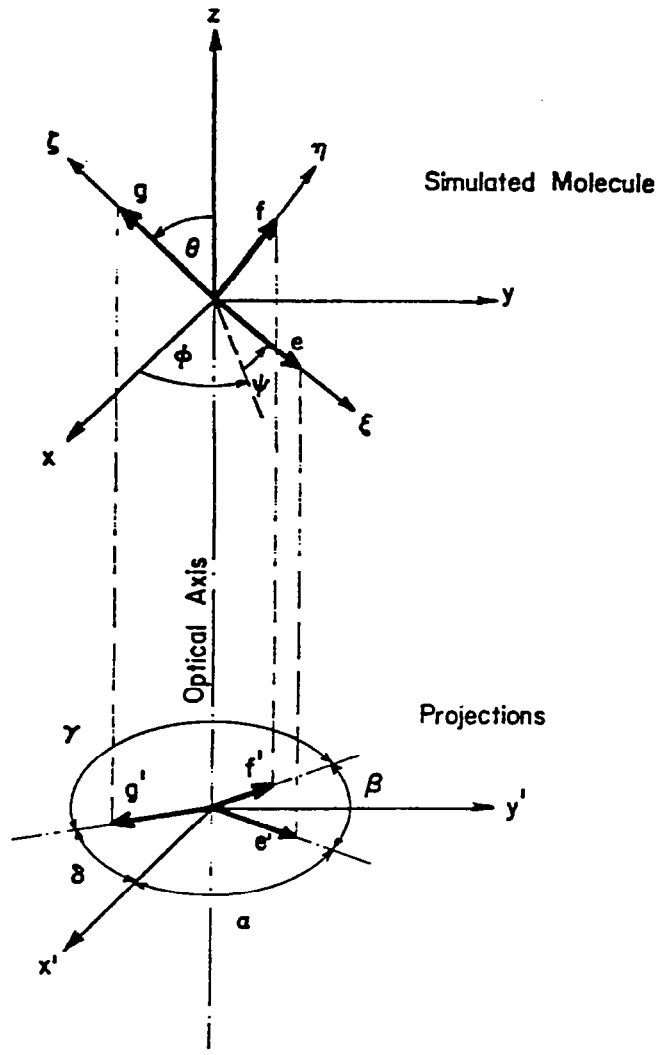

Figure 3.3 Geometrical model for the analysis of molecular orientations. e,f,g are three different transition moments of a simulated molecule in the directions ζ, η, ξ. The coordinate system of ζ, η, ξ is turned by the three Eulerian angles [8] ϕ, θ, χ relative to x, y, z. e', f', and g' are the measured projections of e, f, and g. δ, α, β are the angles of orientation of the transition moments.

In general, the orientation of a three-dimensional body is defined by the Eulerian angles [8]. Therefore, a set of three independent (not collinear and not coplanar) transition moments would define the orientation of a three dimensional molecule in space. Since the experiment tells only the orientation, but not the direction of the transition moments, eight solutions are theoretically possible. Conditions like flow direction and the spatial interrelationship will reduce the number of solutions to one.

Attempts to solve the problem analytically were made. The apparently simple problem yielded a system of nonlinear equations. It seems to be easier to solve the problem on a computer using computer graphics. Rotating a simulated molecule, (Fig. 3.3) consisting of three transition moments, systematically around the Eulerian angles until the projection of the molecule fits best with the maxima of the angular distribution functions will give the solutions. A verification of the solutions will yield the correct molecular orientation. To make it simple, the bonds of the molecule in Figure 3.3 are assumed to be orthogonal. The proposed method will also work for a set of nonorthogonal but independent bonds.

3.3 Michelson Interferometer

3.3.1 Optical Concept of a Michelson Interferometer

The optical diagram of a Michelson interferometer is shown in Figure 3.4. A Michelson interferometer is a versatile

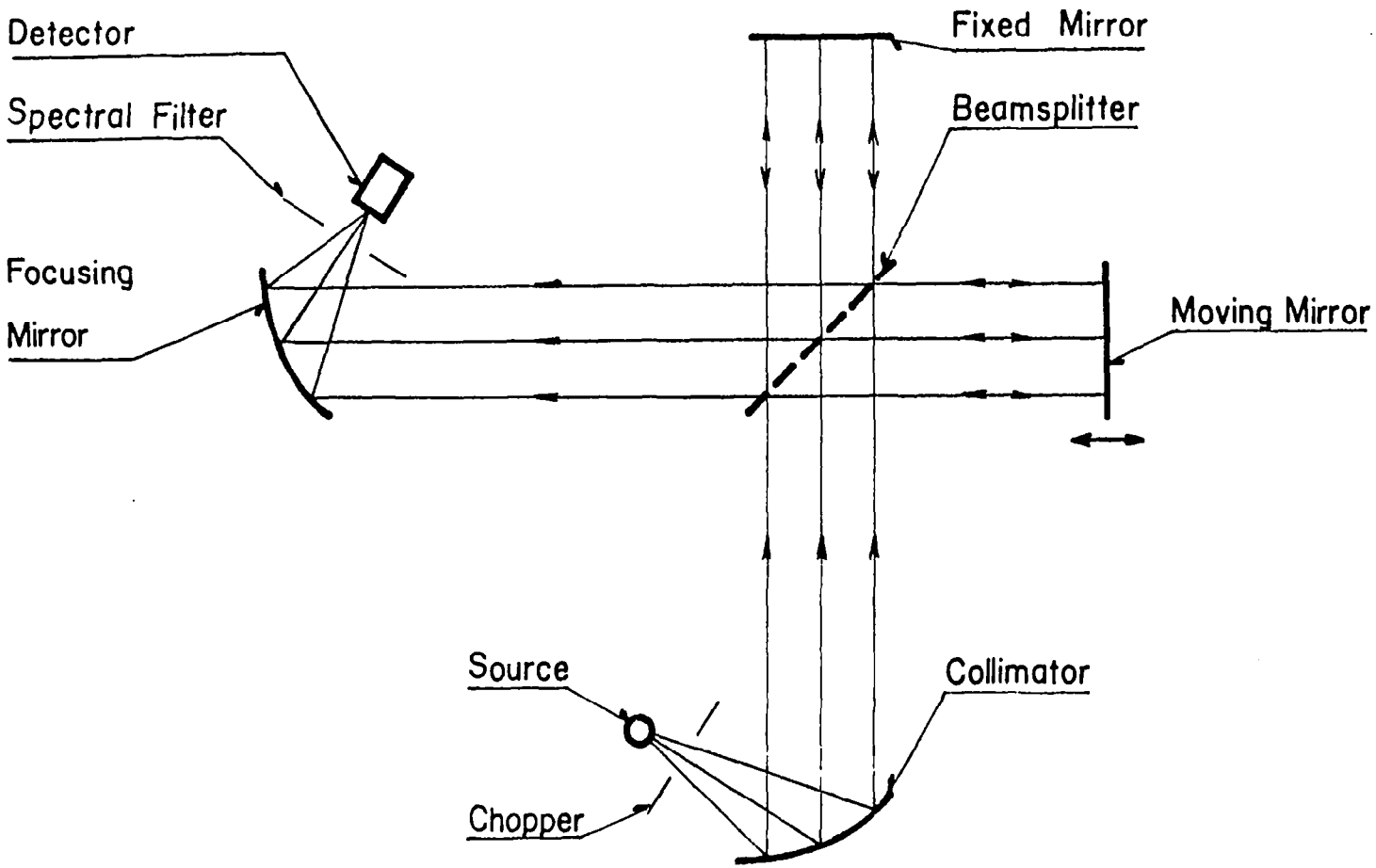

Figure 3.4 Schematic of a Michelson interferometer

instrument but only the spectral analysis, decomposition of radiation in its frequencies, will be treated here. Grating and prism spectrophotometers will convert radiation optically into intensity as a function of frequency. A Michelson interferometer, as any Fourier spectrophotometer, superposes the radiation which can then be unscrambled mathematically. There are distinct advantages, to be explained later, of the second method, which justifies the more complex set up.

The radiation of the source (Figure 3.4) is collected by the collimator. In an emission instrument, the sample is the source. The beamsplitter ideally transmits 50% and reflects 50% of the incoming parallel radiation. Material and film thickness of the beamsplitter are chosen according to the wavenumber region of operation. Both the reflected and the transmitted radiation will be reflected back by a flat mirror, a moveable and a fixed one, to the beamsplitter. The two beams, one retarded by the different path length introduced by the moveable mirror, will be recombined and focused onto the detector. The plot of the signal versus mirror displacement is called the interferogram. The wanted spectrum is the Fourier transform of this function. A short derivation given later will prove the validity of this statement.

3.3.1.1 General advantages of a Fourier spectrophotometer. The detector of a Fourier instrument receives at one time all information from the entire spectral range of a given source whereas a conventional grating or prism instrument receives information only

within a very narrow spectral region at the time given by the observation slit. Therefore the signal detected in a grating instrument by the detector is proportional to the time t of the scan and inversely proportional to the number of spectral elements given by

$$m = \frac{\sigma_2 - \sigma_1}{\delta\sigma} \tag{3.4}$$

for a spectrum recorded between σ_2 and σ_1 with the resolution $\delta\sigma$.

If the noise is random and independent of signal level (assuming a thermal detector), the noise is proportional to $(\frac{t}{m})^{1/2}$. The signal to noise ratio of a grating instrument is therefore:

$$\frac{S}{N}\Big|_G \alpha \left(\frac{t}{m}\right)^{1/2} \tag{3.5}$$

For a Fourier instrument, the signal is proportional to the recording time t and the noise proportional to $t^{1/2}$. The signal to noise ratio is therefore:

$$\frac{S}{N}\Big|_F \alpha\ t^{1/2} \tag{3.6}$$

This predicts an advantage for the Fourier instrument by a factor of $m^{1/2}$. The system used for this work yields a factor of $m^{1/2} = 11$ over a grating instrument with the same resolution and scanning time.

A decrease in resolution, i.e. opening the slit, would improve the signal to noise ratio for a grating instrument; whereas for a Fourier instrument the resolution is given by the maximum mirror

travel and is therefore independent of signal to noise ratio. This effect was first described by Fellgett in his thesis and is now called the Fellgett advantage.

The Jacquinot or throughput advantage states that, for an ideal Michelson interferometer, the throughput is given by the area and the solid angle of the collimator and is constant throughout the whole instrument. But for a grating instrument the throughput is limited by the area of the entrance slit.

3.3.1.2 Short derivation of the basic integral. The amplitude incident on the beamsplitter is defined by

$$E(z,\sigma) = E_o(\sigma)\, e^{i(\omega t - 2\pi z\sigma)} \tag{3.7}$$

After reflection from and transmission through the beamsplitter, the recombined amplitude is

$$E(z_1, z_2\sigma) = rtE_o(\sigma)[e^{i(\omega t - 2\pi z_1\sigma)} + e^{i(\omega t - 2\pi z_2\sigma)}] \tag{3.8}$$

z_1, z_2 are the path lengths of the two arms of the interferometer. The flux for the spectral range $d\sigma$ is (within multiplying constants):

$$\begin{aligned} I(z_1, z_2,\sigma)\, d\sigma &= E(z_1, z_2,\sigma) \cdot E^*(z_1, z_2,\sigma)\, d\sigma \\ &= 2|rt|^2 E_o^2[1 + \cos 2\pi\,(z_1 - z_2)\sigma]\, d\sigma \end{aligned} \tag{3.9}$$

The total flux for any path difference $\delta = z_1 - z_2$ is

$$I_R(\delta) = \int_0^\infty I(\delta,\sigma)\, d\sigma$$

$$= 2|rt^2| \left[\int_0^\infty E_o^2(\sigma)\, d\sigma + \int_0^\infty E_o^2(\sigma)\, \cos(2\pi\sigma\delta) d\sigma\right] \qquad (3.10)$$

The flux for $\delta = 0$ becomes

$$I_R(o) = 4|rt|^2 \int_0^\infty E_o^2(\sigma)\, d\sigma \qquad (3.11)$$

Subtracting half of the flux at $\delta = 0$ from the flux for any path difference gives

$$I_R(\delta) - \frac{1}{2} I_R(o) = 2|rt|^2 \int_0^\infty E_o^2(\sigma)\, \cos(2\pi\sigma\delta)\, d\sigma \qquad (3.12)$$

which is the function for the interferogram.

The cosine transform is defined as

$$F(\sigma) = 2 \int_0^\infty f(\delta)\, \cos(2\pi\sigma\delta)\, d\delta$$

$$f(\delta) = 2 \int_0^\infty F(\sigma)\, \cos(2\pi\sigma\delta)\, d\sigma \qquad (3.13)$$

The spectrum $B(\sigma)$ is proportional to $E_o^2(\sigma)$ using the cosine transform, equation (3.12) can be rewritten:

$$B(\sigma) \propto E_o^2(\sigma) \propto \int_0^\infty \underbrace{[I_R(\delta) - 1/2\ I_R(o)]}_{\text{Interferogram}} \cos(2\pi\sigma\delta)\, d\delta \qquad (3.14)$$

The cosine transform of the interferogram is indeed proportional to the spectrum. Since the amplitudes interfere coherently for $\delta = 0$, the intensity is proportional to the square of the sum of the amplitudes of the electric field

$$I_R(o) \alpha (E + E)^2 = 4E^2 \tag{3.15}$$

For $\delta \to \infty$ the interference will be incoherent

$$I_R (\infty) \alpha E^2 + E^2 = 2E^2 \tag{3.16}$$

Therefore

$$I_R(\infty) = .50 \; I_R(o) \tag{3.17}$$

This relationship is used for the control of the alignment. Instead of the theoretical value of .5, factors between .3 and .4 were achieved.

3.3.2 Polarizer

The polarizer consists of a plate of infrared-transparent TlBr + TlI (KRS-5) on which parallel bands of aluminum were vapor-deposited .4 μm apart. A so-called wire grating polarizer will only work properly if the wavelength is greater than the wire spacing. If an incident electromagnetic wave has its electric vector parallel to the wires, there will be currents induced in the wires and these currents give rise to a reflected wave. This is an ordinary metallic reflection. If on the other hand the electric vector is perpendicular to the grating, no current can flow between the wires. The wave will be transmitted as through a dielectric.

3.4 EHD Contact

The standard hydrodynamic theory fails to predict the film thickness in highly loaded contacts (high load, low speed). The calculated film thickness will be smaller than a typical surface

roughness, despite the fact that such highly loaded contacts (gear roller) actually work. Hydrodynamic theory does not account for the change of lubricant properties and the elastic deformation of the bearing material under high pressure.

Density changes cannot account for a significant change in film thickness. However, viscosity depends strongly on pressure. An empirical pressure viscosity relationship has been established which is sufficiently accurate:

$$\eta = \eta_0 \quad \exp(\alpha p) \tag{3.18}$$

where η is the viscosity in [Pa•s] at pressure p and η_0 the atmospheric viscosity. The unit of α, the pressure viscosity coefficient, is $[Pa^{-1}]$.

High pressure will be present in highly loaded contacts which will lead to a deformation of the bearing material. For a small film thickness compared to the deformation, the pressure distribution in the gap will be close to the Hertzian distribution for a dry contact.

$$p = p_{MAX} \ (1 - r^2/a^2)^{1/2} \tag{3.19}$$

where a is the radius of the contact spot. On the other hand, if the load is small and the speed very high the bearing can be assumed to be rigid (hydrodynamic theory).

3.4.1 Grubin's Theory

Grubin [7] examined in detail the elastohydrodynamic problem. The observation of the formula for the film thickness for two cylinders, considering the influence of pressure on viscosity, rests on two simplifying assumptions:

1. The deformed shape of the cylinders will be the same as that in a dry contact.
2. High pressure is developed in the entry region to the Hertzian zone.

The film thickness becomes

$$\frac{h_o}{R} = 1.95 \frac{(\eta_o \cdot u \cdot \alpha)^{8/11}}{R^{7/11}} \cdot \frac{E'^{1/11}}{P_y^{1/11}} \tag{3.20}$$

where E' represents the elastic properties of an equivalent cylinder near a rigid plane

$$\frac{1}{E'} = 1/2\left(\frac{1 - \sigma_1^2}{E_1} + \frac{1 - \sigma_2^2}{E_2}\right) \tag{3.21}$$

where E and σ represent the modulus of elasticity and Poisson ratio for cylinder 1 and 2, respectively.

The equivalent radius of the two cylinders is similarly

$$\frac{1}{R} = \frac{1}{R_1} \pm \frac{1}{R_2} \tag{3.22}$$

The speed u is given by the average speed of cylinder 1 and 2

$$u = \frac{1}{2}(u_1 + u_2) \tag{3.23}$$

This gives a very accurate representation of the mean lubricant film thickness. Interestingly enough, the influence of speed is much stronger than the influence of the load.

PART 4

APPARATUS

Most parts of the original set-up [2] have been retained. The detection of oriented material required the installation of a polarizer. For the measurement of aircraft fuel line deposits, the necessary increase in resolution and sensitivity was expected to be achieved by (i) a lens with a larger numerical aperture and magnification, (ii) a blackbody reference with temperature and aperture separately adjustable and (iii) the optional substitution of the tuning forks by a rotating polarizer. Therefore the emission module of the Michelson interferometer was redesigned and a procedure for the proper alignment was developed.

This part contains a detailed description of the designed parts, the possible modes of operation, the initial testing, the other apparatus used in this study and the materials used. An overview of the system is given first.

4.1 Overview of the System

The apparatus consists of a sample holder, a Michelson interferometer with a special inlet system and the necessary peripherals (Figure 4.1).

The radiation from the heated sample is collected by a microscopic lens and fed into the Michelson interferometer. The interferometer splits the incoming radiation into two parts and recombines them after one beam passes through an optical

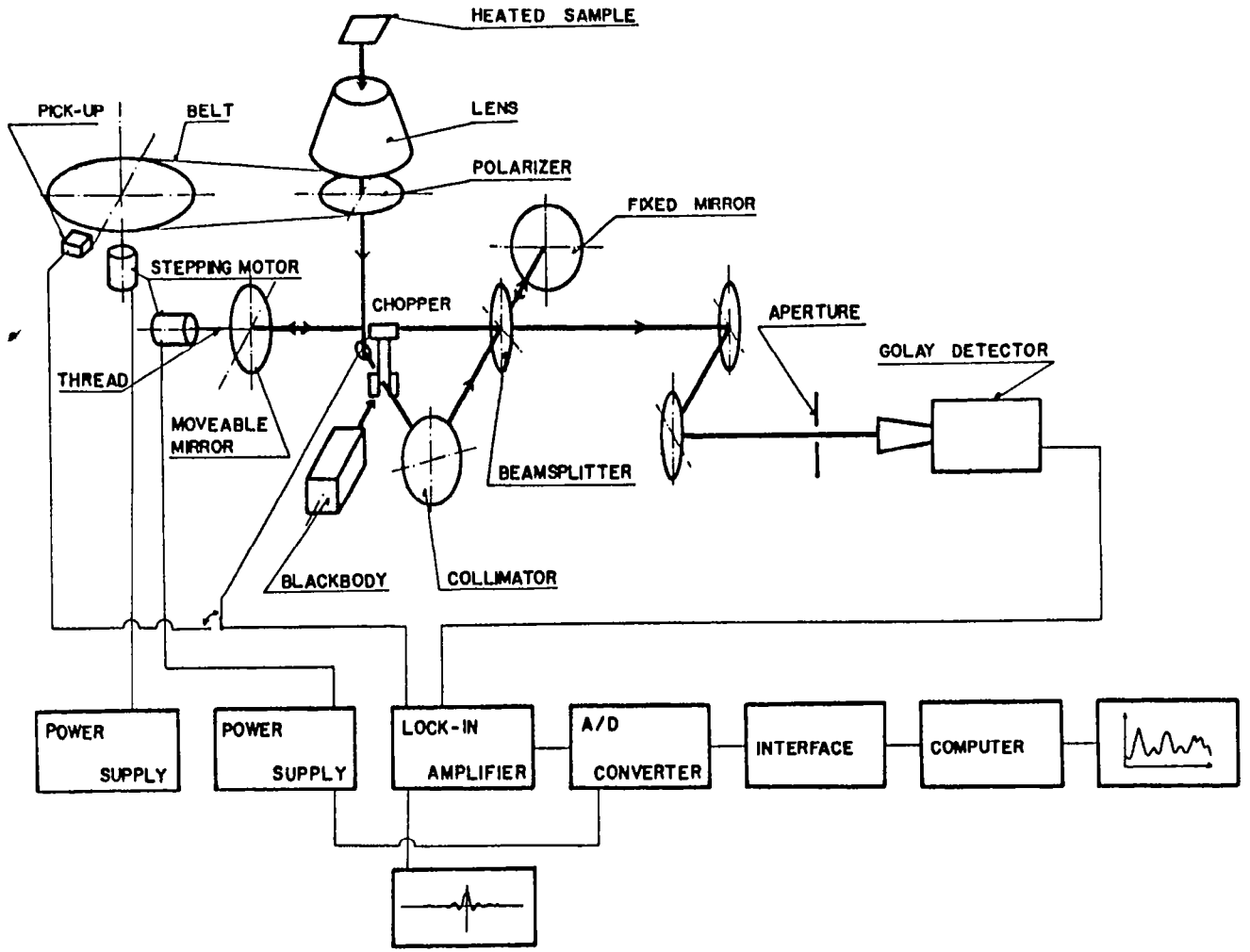

Figure 4.1 Schematic of the infrared emission Fourier microspectrophotometer

path of variable length. The detector, a pneumatic Golay Cell, transduces the filtered infrared radiation into an electrical signal, which is amplified by a lock-in amplifier and referenced to the chopping frequency. The plot of the amplified detector signal versus path difference or mirror displacement is called the interferogram and is used for control purposes. The actual signal is, after conversion into a digital signal, stored on a floppy disk in the computer. The Fourier transform of the interferogram yields the wanted spectrum. This operation and the plotting of the spectrum are done in a separate run on the minicomputer.

4.2 Newly Designed Parts

The changes and supplements necessary to transform a commercial infrared absorption instrument into an infrared emission (Beckmann FS720) Fourier microspectrophotometer are described here. The concept of the conversion was taken from [2], which means a transformation of the original source module into an emission module. Two conversions were actually carried out. The two versions differ in the type of box used. The first version* installed in the original module box had inadequate space. The second box** was designed as a whole new module. It has more internal space and O-ring sealed panels.

In addition, the beamsplitter holder, the mirror drive and

*based on a commercial instrument donated by the DuPont Company
**based on a commercial instrument donated by the Sun Oil Company

a sample holder system including a stage were designed, constructed and tested. The descriptions of the sample holder and emission module refer to the second version with the totally rebuilt module.

4.2.1 Sample Holder

Two basically different types of samples can be analyzed in the system. The so called "dynamic samples", a simulated ball bearing contact [2] for the study of different fluids in the Hertzian area, are briefly mentioned at the end of this part. The "static samples", materials of mainly organic nature, which can be in the liquid or solid state adsorbed or as a coating on a substrate, are treated in this section.

Emission spectroscopy requires a temperature difference between sample and detector. Typically, a temperature difference of 10 to 15°C is required in our setup for an adequate signal level. To avoid reabsorption of the emitted radiation within the sample, it has to be at constant temperature. In earlier designs the sample was heated from the back and the top was covered by a KCℓ window. Even with these precautions, absorption occurred. The new design features shaped a heated window. A large water mass is kept at constant temperature and is pumped through the heating block and around the window. The same temperature source can also be used to generate a graybody reference radiation at that particular temperature. Several sample holders for differently shaped samples have been designed and tested. All of these holders can be mounted in a X,Y,Z stage with a large size turntable.

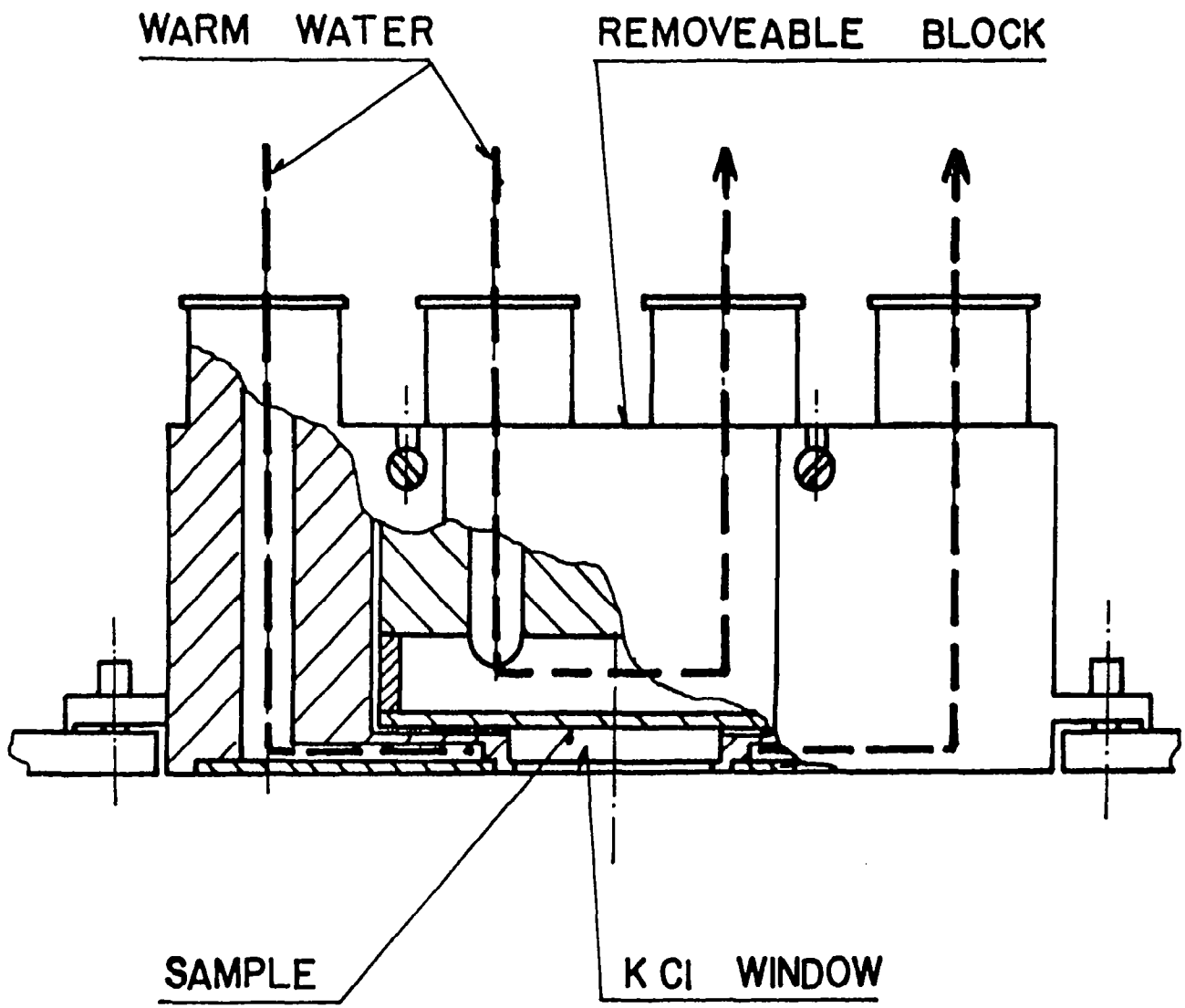

Figure 4.2 Cross-section of sample heat for shims

4.2.1.1 Sample holders. Three holders were made; a general purpose heater, a heater for fuel deposits on shims and a heater for fuel deposits on tubes. Figure 4.2 shows a cross-section through the general propose heater. The heater for fuel deposits on tubes is designed somewhat differently because the geometry of the sample prohibits a window. The unheated area was minimized and well protected by lips.

4.2.1.2 Stage. This stage has six degrees of freedon. The maximum translation in X direction is 160 mm, in the Y and Z directions it is 82 mm. The large turntable of 165 mm inner free diameter can be rotated 360° degrees. The other two rotational degrees of freedom are for alignment purposes only. The turntable features a fine adjustment and a blocking mechanism.

4.2.1.3 Hot Water System. The system is designed to accept up to three users simultaneously. A schematic drawing of the system is given in Figure 4.3. The immersion unit heats, stirs and controls the temperature of the 20 liter water tank. The heating fluid is circulated by a pump in a separate system through the water tank and the sample. This heating fluid is collected in an expansion volume and contains a corrosion inhibitor. The water tank and the expansion volume are well insulated and enclosed in a wooden box on wheels.

4.2.2 Emission Module

The emission module replaces the original source module of

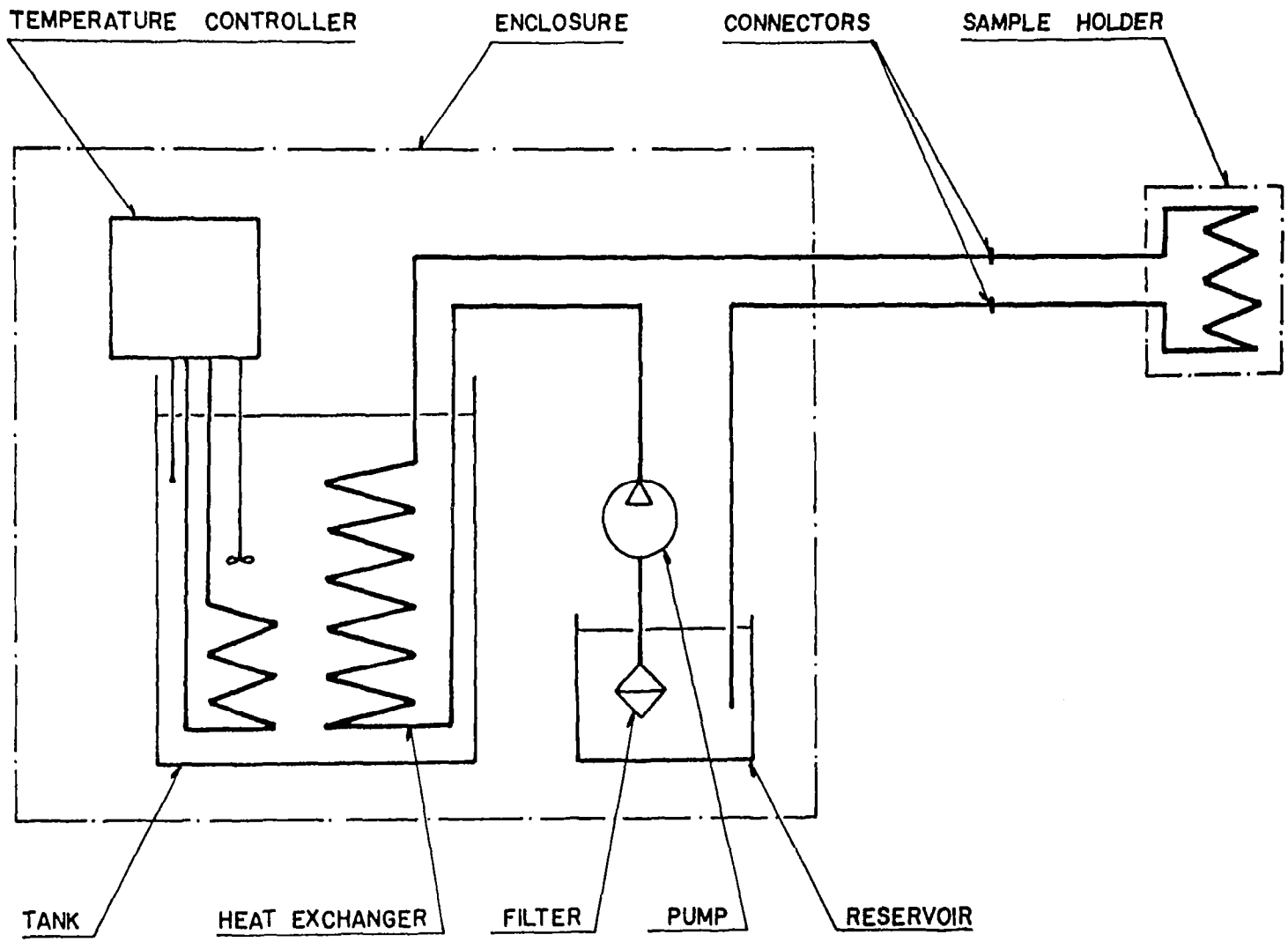

Figure 4.3 Schematic of hot water system

of the commercial instrument. This new module contains the following major optical elements:

- lens and lens holder
- drive for polarizer
- holder for 45° mirror
- tuning forks with holder
- blackbody temperature reference
- collimating mirror (off-axis paraboloid).

All elements except the collimating mirror contained in the source module have been redesigned. The optical concept is identical with King's apparatus [2] except for the polarizer driven between lens and mirror holder. The whole unit was designed to be filled with dry nitrogen instead of air. Two removable panels allow easy access to the parts built into the module.

4.2.2.1 Lens and Lensholder. The system is designed to accept any standard microscope objective. Only reflecting microscope lenses are used because of their large working distances and their achromaticity. The objective seating plane (top surface of lens holder) is at a distance of 150 mm from the focal point of the off axis paraboloid mirror. Experiments showed that the "tube length" is not critical. Therefore no translation of the lens in the direction of the optical axis is built in the holder. The only possible translations of the stage, to allow the centering of the lens, are in the plane perpendicular to the optical axis.

4.2.2.2 Rotating Polarizer. The principal change of the optical instrumentation centers around the optional substitution of the radiation chopper by a rotating polarizer. The ideal location of the polarizer would be between the sample and the microscope objective because then radiation from extraneous downstream parts is not detected. The working distances and the need for a KCl window in front of the sample (see 4.2.1) prohibit this version. Hence we put the polarizer after the lens. The turning polarizer requires a new mechanism to generate the reference signal for the lock-in amplifier and a means to adjust the phase between the reference signal and the orientation of the polarizer.

The actual design is shown in Figure 4.4. The polarizer, an infrared-transparent TlBr + TlI (KBR-5) disk, coated with bands of aluminum 0.4 μm apart, is driven by a stepping motor over a 2:1 timing belt drive. The possible future control of the whole system by a computer has led to the use of a stepping motor. The checkered wheel, mounted on top of the gear, driven directly by the motor, generates together with the lamp/photocell pick-up the reference signal for the lock-in amplifier. Shifting the pick-up relative to the polarizer allows the observation of the sample at a different angle. A scale engraved on the big gear allows a well defined rotation of the polarizer when the motor stands still. A precision miniature timing belt links the two gears. The smaller gear is rotating concentric to the optical axis and is mounted on the hollow shaft which is supported by two ball bearings. The polarizer is carefully mounted in a special holder which fits into the steps of the shaft. The holder is secured against rotation relative to the shaft by a pin slit arrangement.

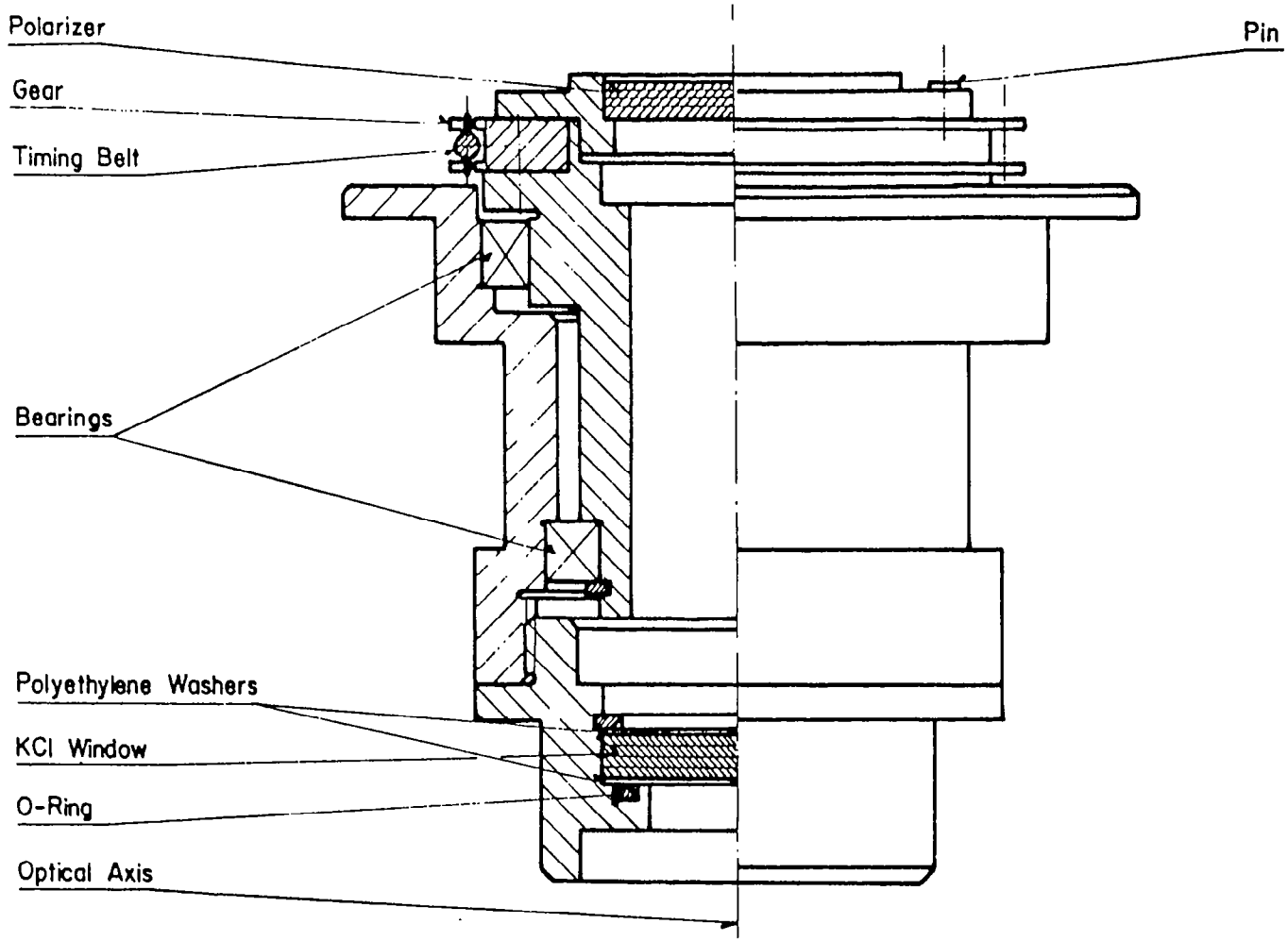

Figure 4.4 Cross-section of polarizer drive

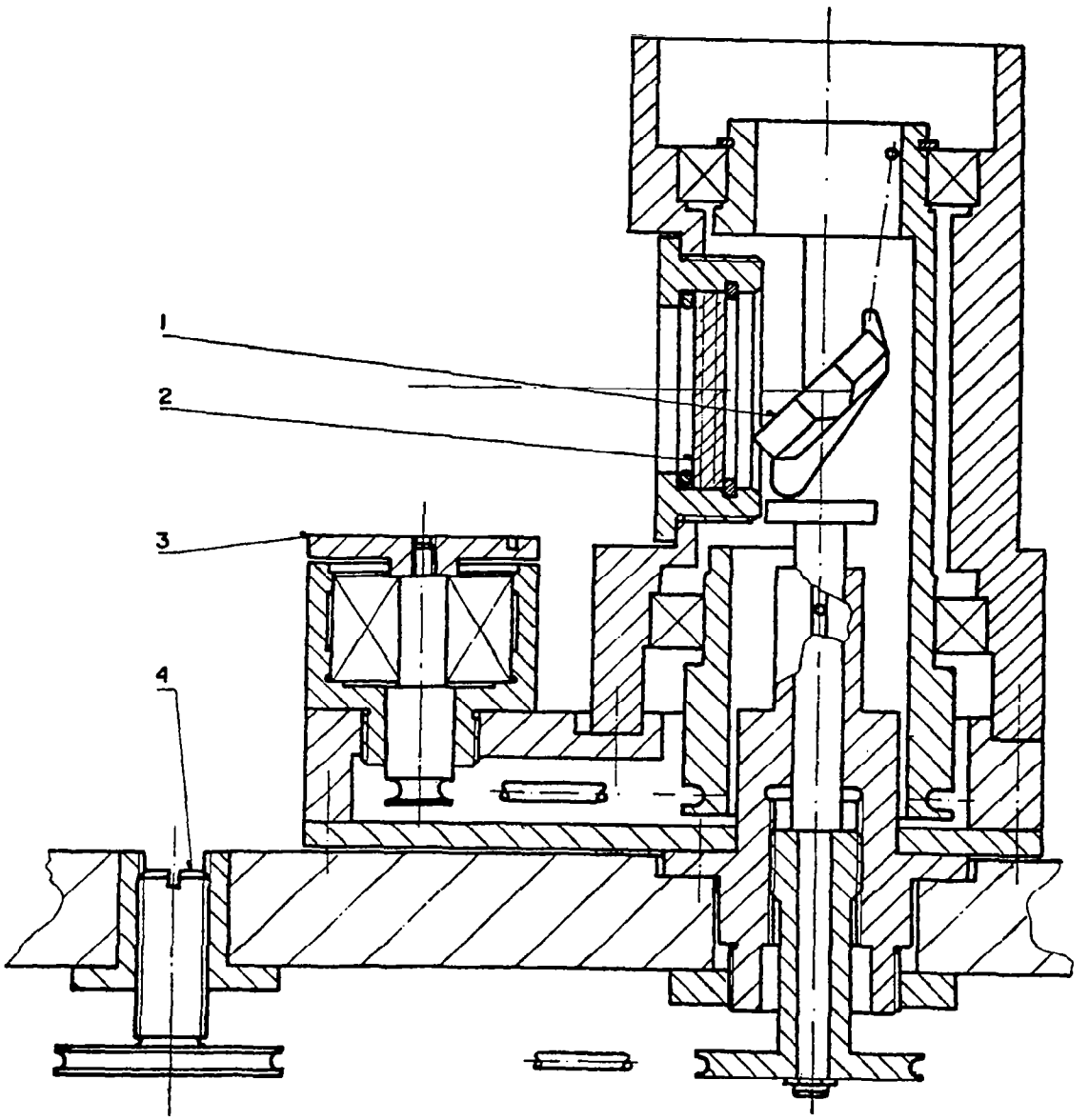

Figure 4.5 Cross-section of 45° mirror holder. 1) reflective surface 2) KCℓ window, 3) adjustment of yaw, 4) adjustment of tilt

The emission module had to be a sealed unit. A KCℓ window was therefore inserted into the adapter between the ball bearing housing of the polarizer drive and the 45° mirror housing. This location of the window allows a simple seal. At other locations, rotating shafts would have to be sealed too.

4.2.2.3 45° Mirror Holder. The mercury arc source of the original commerical instrument was smaller than the emission inlet system. To accommodate the extra room needed, the emitted infrared radiation is therefore deflected by 90° at the so-called 45° mirror and fed into the original optical path. Two rotational degrees of freedom are necessary for the 45° mirror to interface the off-axis paraboloid mirror properly with the microscope objective.

The design is shown in Figure 4.5. The 12 mm diameter gold-coated mirror is mounted in a hollow shaft by two cone-shaped screws, which allow a rotation of the mirror around a horizontal axis. The shaft is supported by two ball bearings pressed into the housing of the mirror holder. An O-ring belt drive linking the shaft and a special screw, allows the adjustment of the yaw with a screwdriver from the outside of the instrument. A piston, moved by a transportation thread which is also driven by an O-ring belt, slides on the cam soldered at the mirror holder. The adjustment of the tilt can also be done with a screwdriver from the outside. The arrangement by which the cam is sliding on top of a piston allows the orthogonal adjustment of the yaw and the tilt. The top end of the housing fits into the adapter between the polarizer and the 45° mirror holder. The entire holder is mounted with one screw on

the frame hung on the top cover plate of the emission module. An oversized clearance hole allows the proper alignment of the pile consisting of the polarizer drive, the adapter and the 45° mirror holder. At the exit of the optical path, a KCℓ window (22 mm diameter, 4 mm thickness) or an aperture can be mounted. This option is presently not used. The window is also very useful for the initial alignment of the instrument.

4.2.2.4 Tuning fork with holder. The Golay Cell, a differential device, requires a chopped signal. This is done between the 45° mirror and the collimator by a commercial tuning fork. At this location it is possible to feed a temperature reference into the optical path, when the sample beam is blocked.

The natural frequency of the tuning fork is 13 Hz (DuPont interferometer) and 20 Hz (Sunoco interferometer). The forks are excited by electromagnets driven by a special electronic oscillator. This device also produces the reference signal for the lock-in amplifier. At the two ends of the fork, highly reflective blades are mounted. They overlap at the minimum position and are about 10 mm apart at the maximum position.

The holder allows a proper alignment of the chopper. The sample radiation has to pass in the center between the opened blades. The reference beam has to be reflected by the closed blades and fed into the system. For this purpose yaw, tilt and the distance of the chopper to the 45° mirror holder can be adjusted

4.2.2.5 Blackbody Reference Source. When the infrared emission of the irregular surfaces is scanned, the principal obstacle to good spectral contrast is the large contribution of scattered radiation and background radiation from substrates with a high emissivity, which may cause a strong graybody radiation. Most of the scatter comes from surface irregularities. To reduce the relative contribution of the graybody radiation one can use, besides a polarizer and/or a small field of view microscope objective, a blackbody. For optimum spectral quality the blackbody temperature has to be matched to the sample temperature as closely as possible and the radiant flux has to be adjustable continuously.

The blackbody reference source (Figure 4.6) consists of (i) a cavity which can be heated or cooled, (ii) a continuously adjustable radiant flux and (iii) a controllable outer surface temperature. The central cavity, a brass cylinder with an axial bore, can be heated by two different means. Three 20 Watt miniature cartridge heaters can be applied for samples not heated by the hot water system described in 1.2.1. Quick cooling is achieved by flushing cold water through the inner cooling circuit. For samples heated by the hot water, the inner cooling circuit can be hooked up to the hot water system. A wedge-shaped aperture, remotely controlled, allows the adjustment of the radiant flux for a given cavity temperature.

The outer surface is kept at a constant, preselectable temperature--even in an enclosure--by the outer cooling system. The coolant is provided by a system similar to the hot water system but, instead of the temperature controller, a simple ice bath is used. Three thermocouples are installed. Two thermocouples measure the temperature of the cavity, the third measures the outer surface temperature.

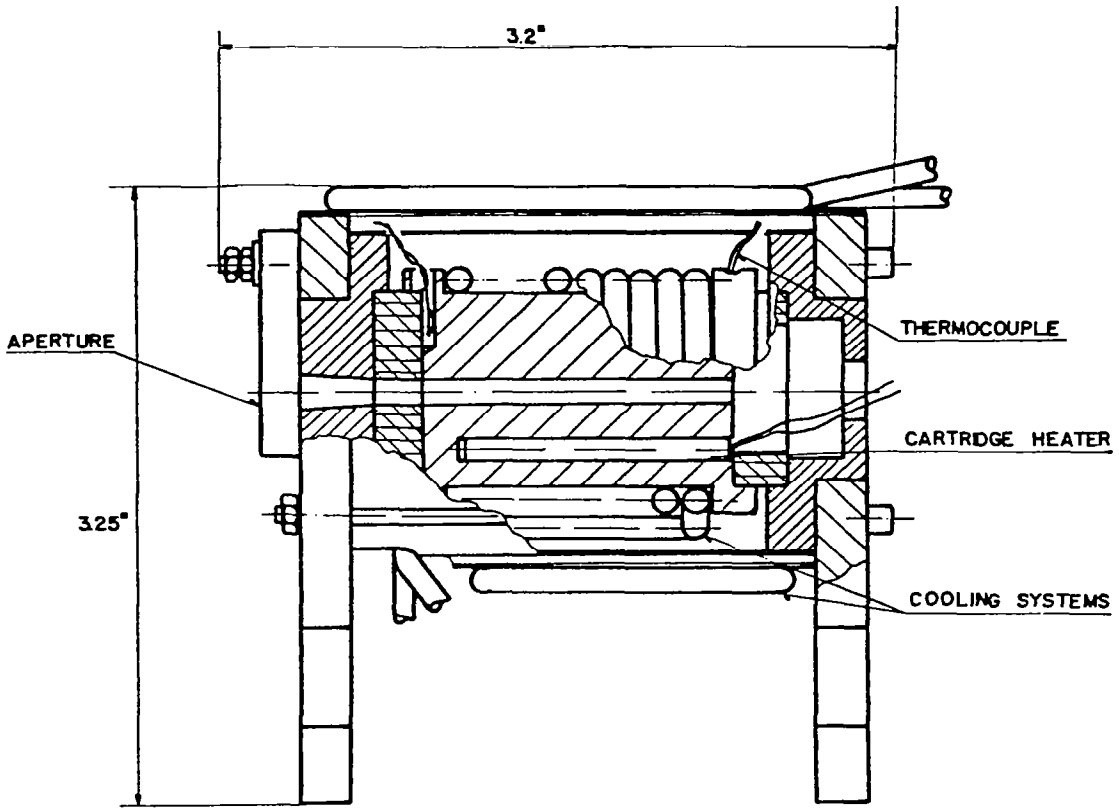

Figure 4.6 Cross-section of blackbody reference shown in Figure 4.12a

4.2.3 Mirror Drive

The original mirror drive allowed a minimum mirror movement of 2.5 μm per step. An optical path difference of 1 μm or a mirror displacement of 0.5 μm is required to allow the collection of data in the 0 - 5000 cm^{-1} wavenumber range which is selectable by optical filters. A timing belt driven gear was therefore inserted between the stepping motor and the micrometer screw of the original mirror drive.

The possibility of an essentially backlash- and maintenance-free operation of a timing belt-driven gear compared to a two stage gear box led to this particular design. Proper belt tension is achieved by an eccentric screw which can be set at any position.

4.3 Modes of Operation

Three modes of operation are defined for the micro-spectrophotometer. The system contains two chopping devices; the tuning fork and the rotating polarizer, which have to be used alternatively. Mode 1 operation, the standard way of running the instrument, uses the tuning fork only. In Mode 2 operation, the rotating polarizer chops the infrared emission. Mode 3 operation uses the tuning forks, but the polarizer is inserted and not rotating. Table 4.1 gives an overview of the three modes.

4.3.1 Mode 1

Under Mode 1 operation (Fig. 4.7) the polarizer is removed and the differential signal ($I - I_b$) corresponds to the difference of sample and blackbody radiation, which are alter-

Table 4.1 Modes of operation

MODE	CHOPPER	REFERENCE	DIRECTION DETECTION
1	Tuning Fork	Blackbody with Aperture	——
2	Turning Polarizer	Internal	Phase to Reference Signal
3	Tuning Fork	Blackbody with Aperture	Static Polarizer

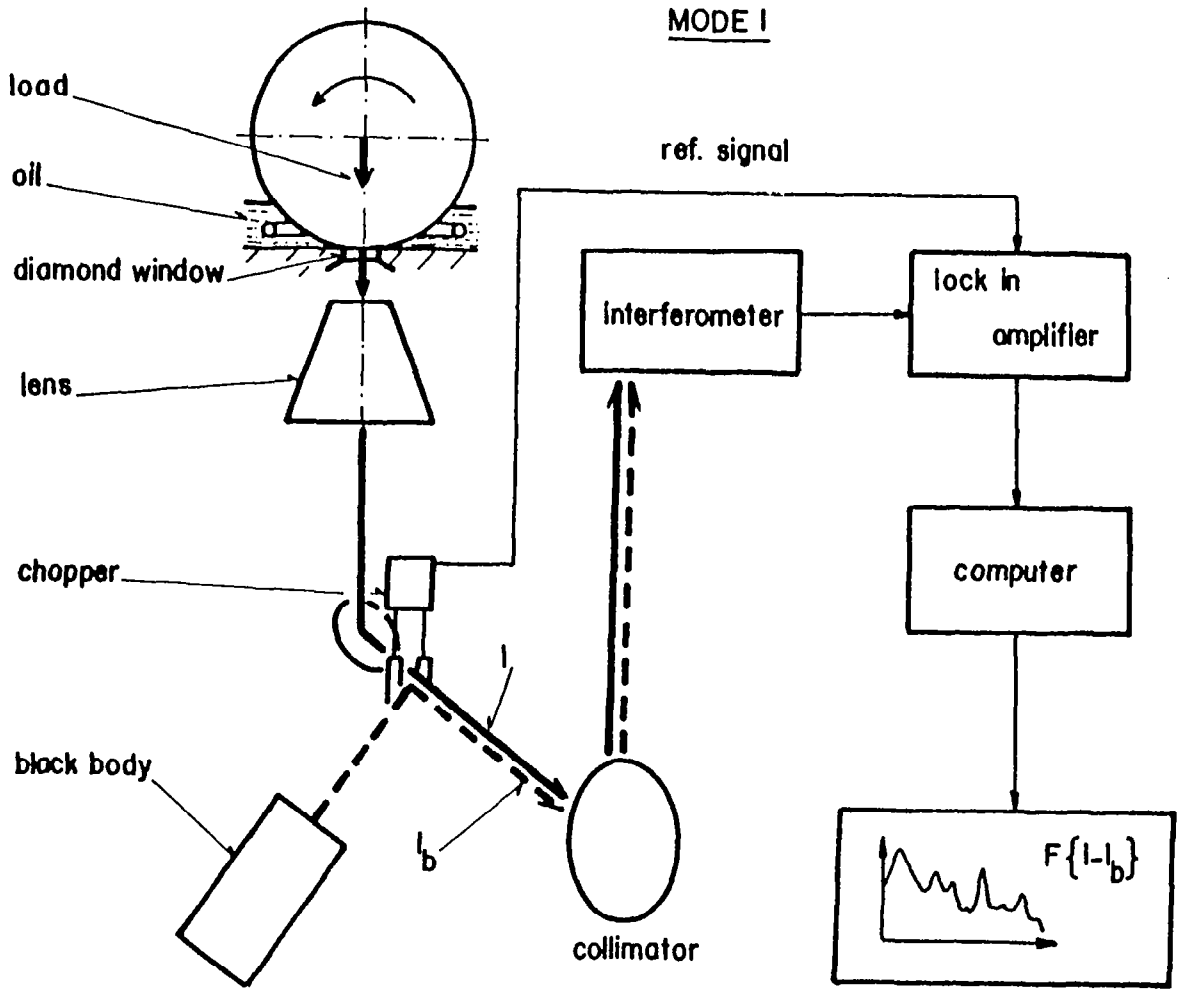

a) NO POLARIZER

Figure 4.7 Mode 1, operation with chopper and blackbody reference giving spectra representing the difference between source planes of polarization

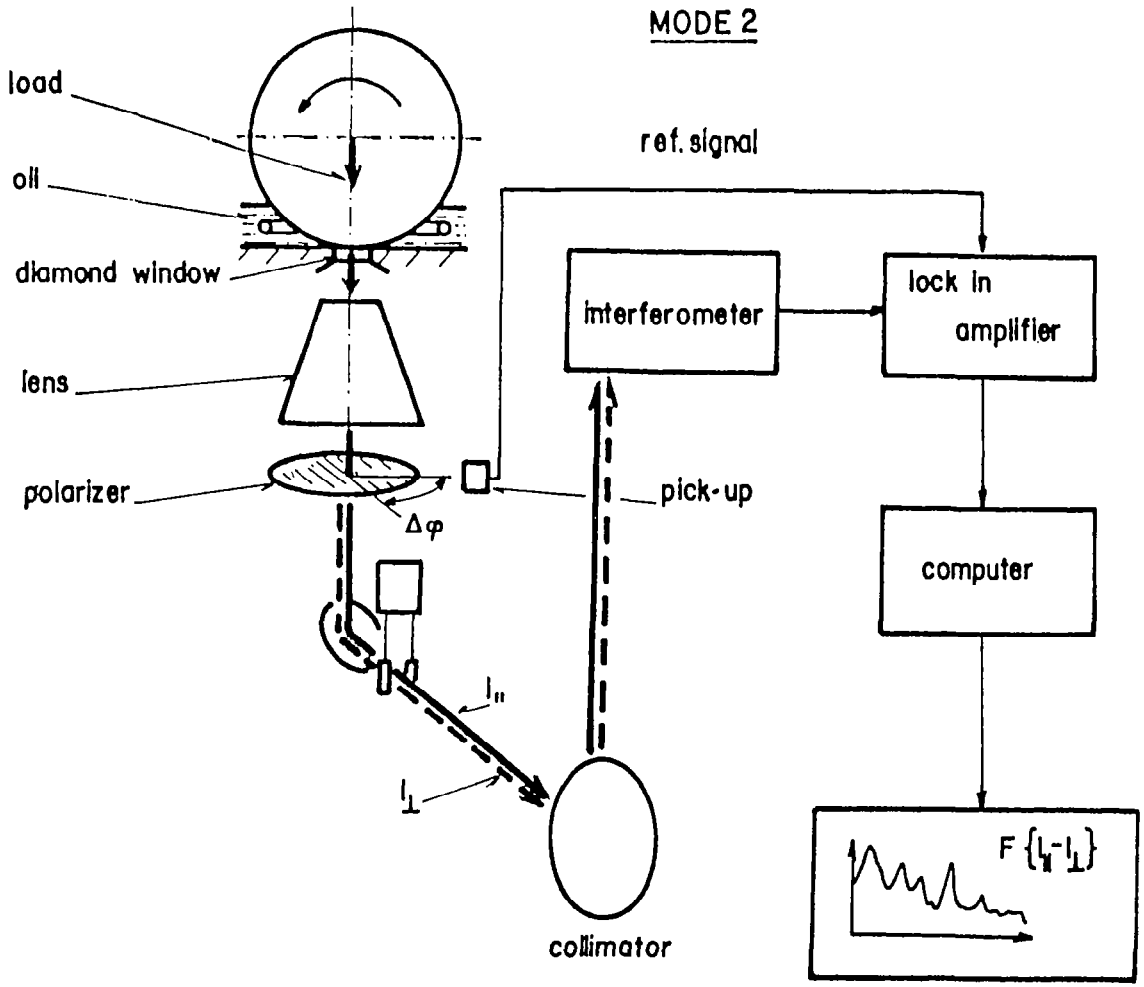

b) ROTATING POLARIZER

Figure 4.8 Mode 2, operation with rotating polarizer, giving spectra representing the difference between two perpendicualr planes of polarization

natingly reflected into the interferometer by the chopper tines. The lock-in amplifier is referenced to the frequency of the tuning forks.

4.3.2 Mode 2

Under mode 2 operation (Fig. 4.8) the tuning forks are not operational. The polarizer is rotating at constant speed, the angular speed being half that of the chopper frequency. The differential signal is the difference of intensities between radiation polarized parallel and perpendicular to the reference plane. This mode provides dichroic spectra. The reference signal is generated by a lamp/photocell pick-up above a disk attached to the pulley, which is painted with white and black sectors. The reference plane is defined by the initial orientation of the polarizer relative to the lamp/photocell pickup and the phase setting of the lock-in amplifier. Therefore shifting of the pick-up relative to the polarizer allows the observation of the sample at different angles relative to the reference plane.

Mode 2 operation provides the maximum sensitivity since randomly polarized blackbody or graybody radiation is eliminated. It also provides proof of polarization or alignment of the dipolar transition moment causing the observed infrared emission bands and, conversely, permits determination of the orientation of the molecular species of the sample from which these bands originated. Mode 2 operation is limited to polarized bands, i.e. not to the combination frequencies ascribable to a number of transition moments of multitudinous orientations. Since the Mode 2 spectra are dichroic spectra--

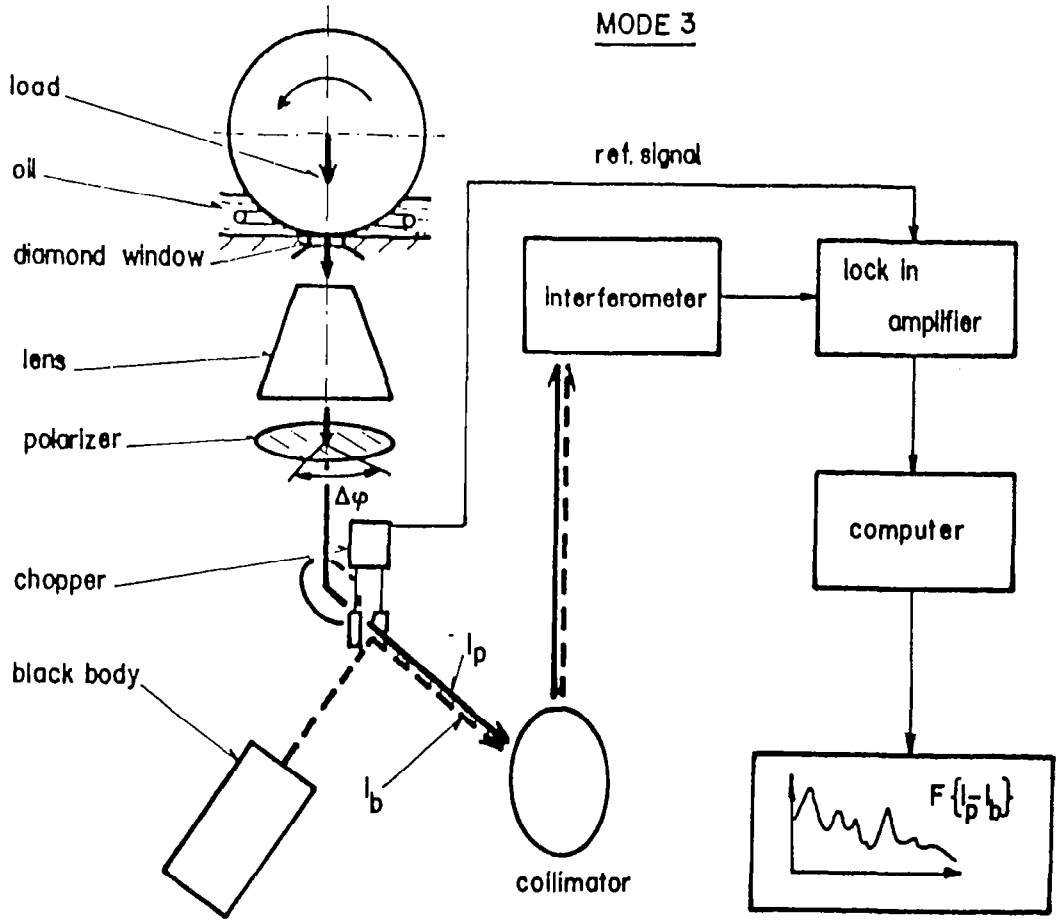

c) STATIONARY POLARIZER

Figure 4.9 Mode 3, operation with chopper, blackbody reference, and a polarizer in a fixed position

representing differences of emission intensities parallel and perpendicular to the reference plane--series of spectra are required for the interpretation, as will be shown.

4.3.3 Mode 3

Mode 3 operation (Fig. 4.9) is the same as Mode 1 operation except that the polarizer is inserted into the optical path but not rotating. The orientation of the polarizer can be set at any angle with respect to the reference plane. This allows the inspection of a sample at different angles relative to the reference plane. If the reference plane, as defined in the description of mode 2 operation, and the reference plane in mode 3, given by the indicator for the angle of rotation mounted near the checkered pulley, coincide, then comparison of Mode 2 and Mode 3 spectra is possible.

Mode 3 operation, i.e. spectroscopy of radiation polarized in one particular plane and referenced to a standard blackbody, provides spectra that are more easily interpreted than those of Mode 2, but requires at least twice as many experiments for the determination of dichroism and is less sensitive.

4.4 Initial Testing

Before actual research with the instrument could be done, extensive testing was carried out. The spectral accuracy was examined by comparing a grating absorption spectrum with an emission spectrum. Most importantly, the expected increase in resolution

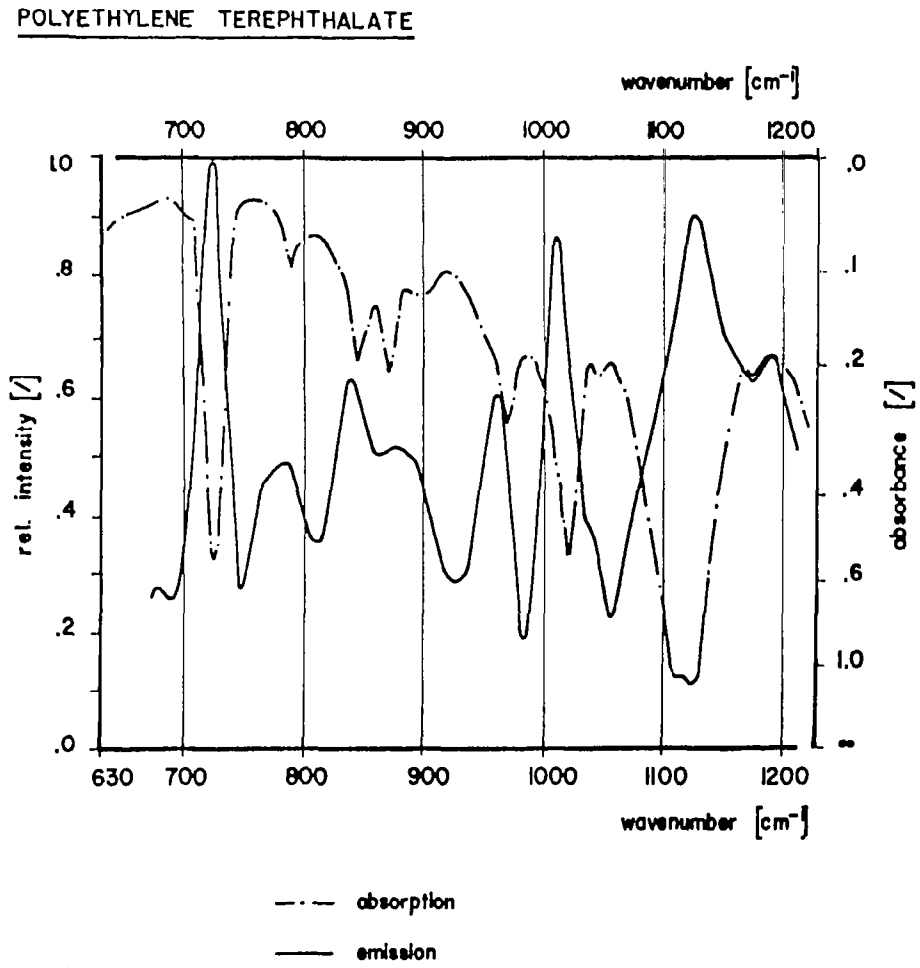

Figure 4.10 Comparison of emission and absorption spectra of a film of polyethylene terepthalate

and sensitivity by the introduction of the rotating polarizer, the blackbody and the lens with the larger numerical aperture had to be verified.

4.4.1 Comparison of Absorption and Emission Spectra

Figure 4.10 shows a comparison of a grating absorption spectrum of a 2.5 μm thick film of polyethylene terephthalate with an (Mode 1) emission spectrum of the same film pressed against the aluminum holder at 35°C. The correspondences in frequency are very good but the relative intensities vary. These variations could be partly due to different spectral resolutions--although the effective slit widths were similar--and partly to polarization (no radiation is emitted along the axis of the dipole transition moment corresponding to a particular infrared band).

4.4.2 Lens with Larger Numerical Aperture

Substitution of a 36X reflecting microscope objective for a 15X objective changes the numerical aperture from 0.28 to 0.50 or the acceptance half-angle from 15 to 30° degrees. Because of the Cassegrainian construction of these objectives, the overall intensity should increase for the higher numerical aperture (N.A.) as the proportion of obstructed central area decreases from 17.5% to 12.5%. This should be the only effect of the N.A. change, since a decrease of field of view almost exactly compensates for the increase of N.A. Furthermore, the spectral contrast (baseline emission bandstrength to background ratio) should increase because of the increased optical thickness of the layer along the average

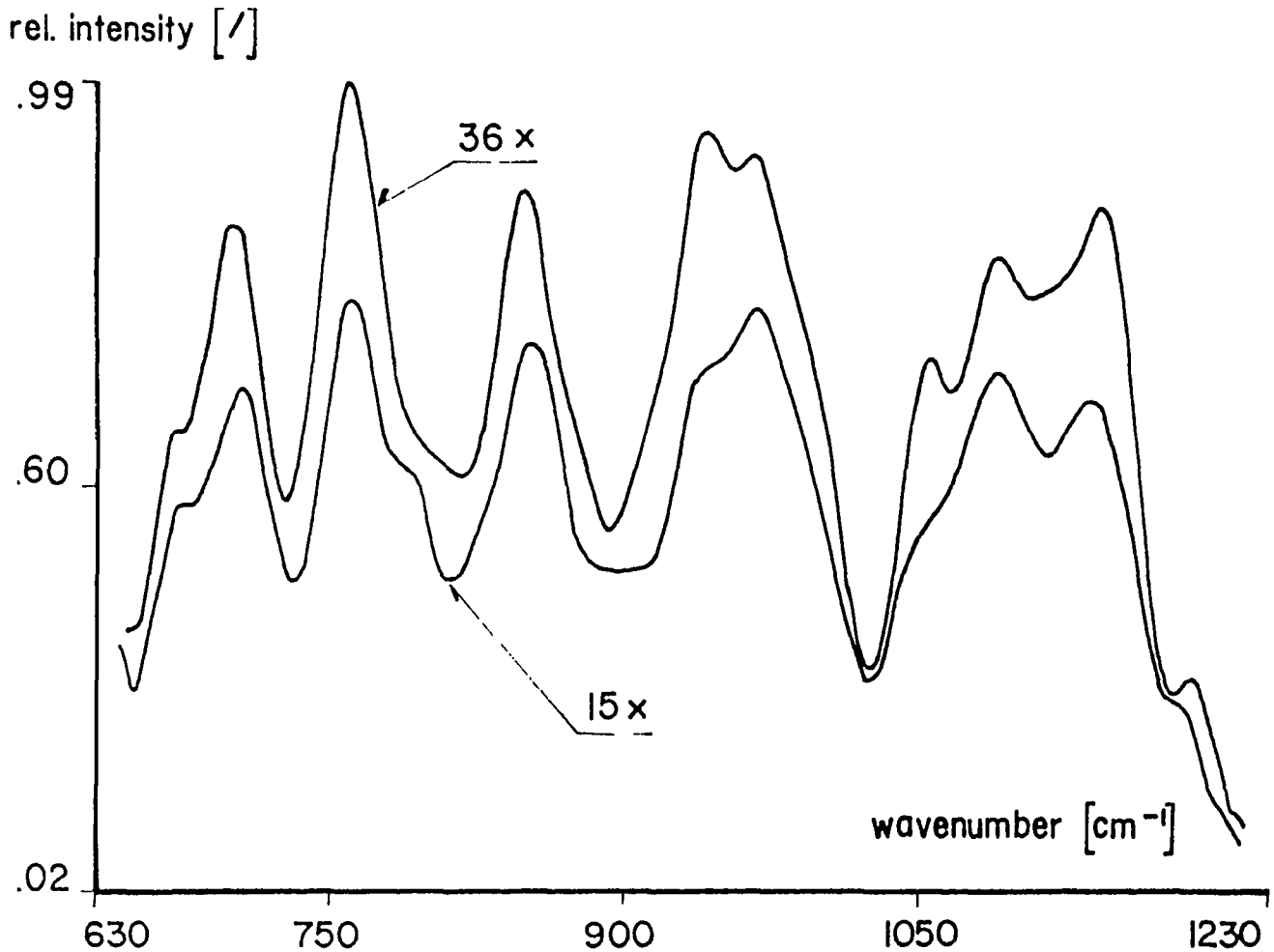

Figure 4.11 Comparison of spectra of a polyphenyl ether coating scanned with microscope objectives of different magnification and numerical aperture

line of sight. Figure 4.11, showing spectra of a layer of a polyphenyl ether liquid on aluminum at 35°C, would seem to be consistent with these assertions. No differences of band intensity enhancements are shown for different bands because the layer was too thick to observe interactions between infrared radiation reflected by the substrate and molecular dipole radiations (e.g. standing wave interactions).

4.4.3 Effect of Blackbody Reference

For optimum spectral quality in Mode 1 operation the blackbody should be matched to the sample temperature and flux as closely as possible. This effect was demonstrated with the same sample of polyphenyl ether adsorbed on aluminum at 35°C, which was used to show the effect of the numerical aperture of the lens (Fig. 4.11). Figure 4.12 shows the spectra with and without the use of the blackbody. The need for the blackbody is obvious.

4.4.4 Mode 2 Operation

Polyethylene terephthalate, an oriented material, was used for verifying Mode 2 operation. Figure 4.13 shows several superimposed spectra recorded with different phase angles. The spectral constrast of Mode 2 is greatly improved compared to the Mode 1 data. Small bands that are not visible under Mode 1 condition will be resolved in Mode 2 even in the neighborhood of strong bands as shown in Figure 4.13 for the 1120 cm^{-1} region. Slight imperfections in the alignment of major bands are due to the fact that a spectrum is the superposition of bands and therefore the maxima of the bands are not

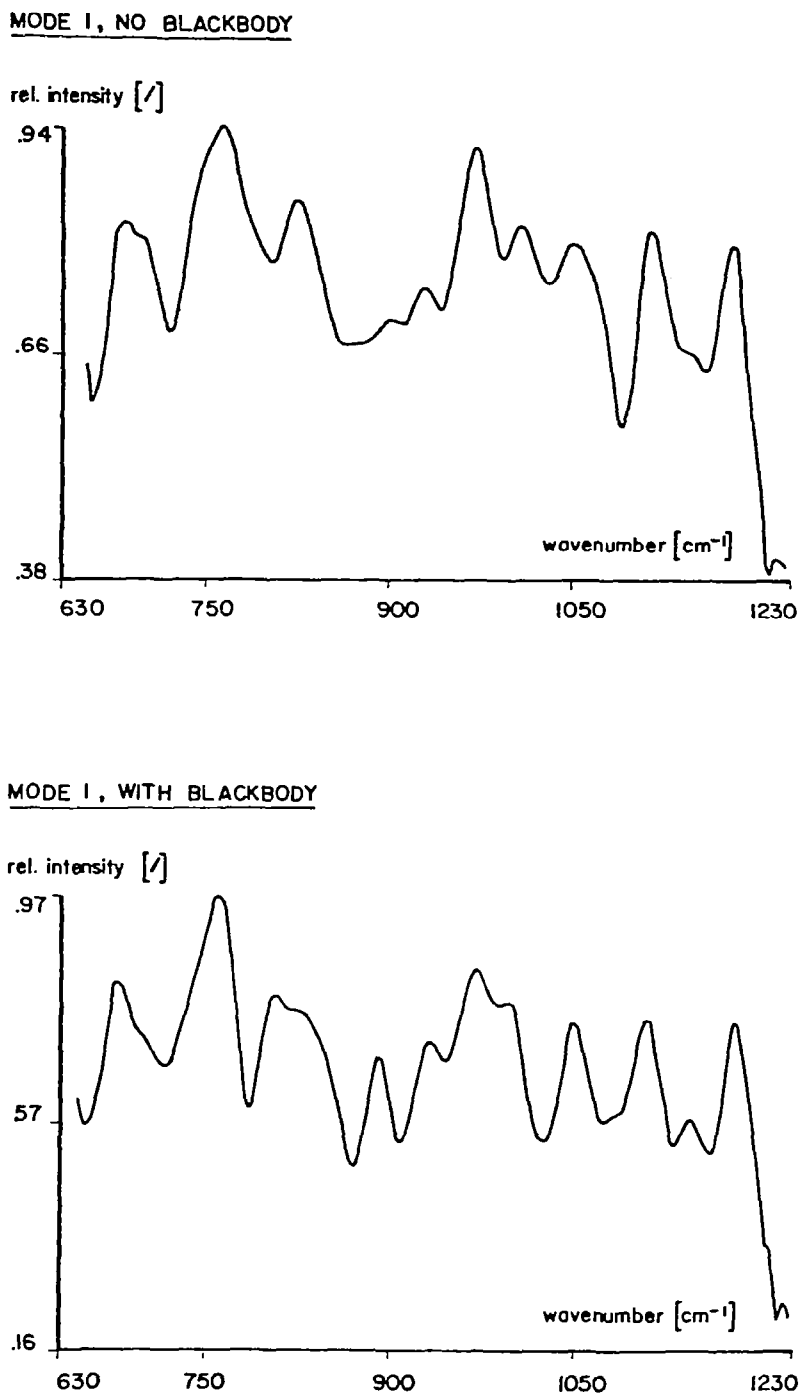

Figure 4.12 Effect of blackbody reference on spectral quality

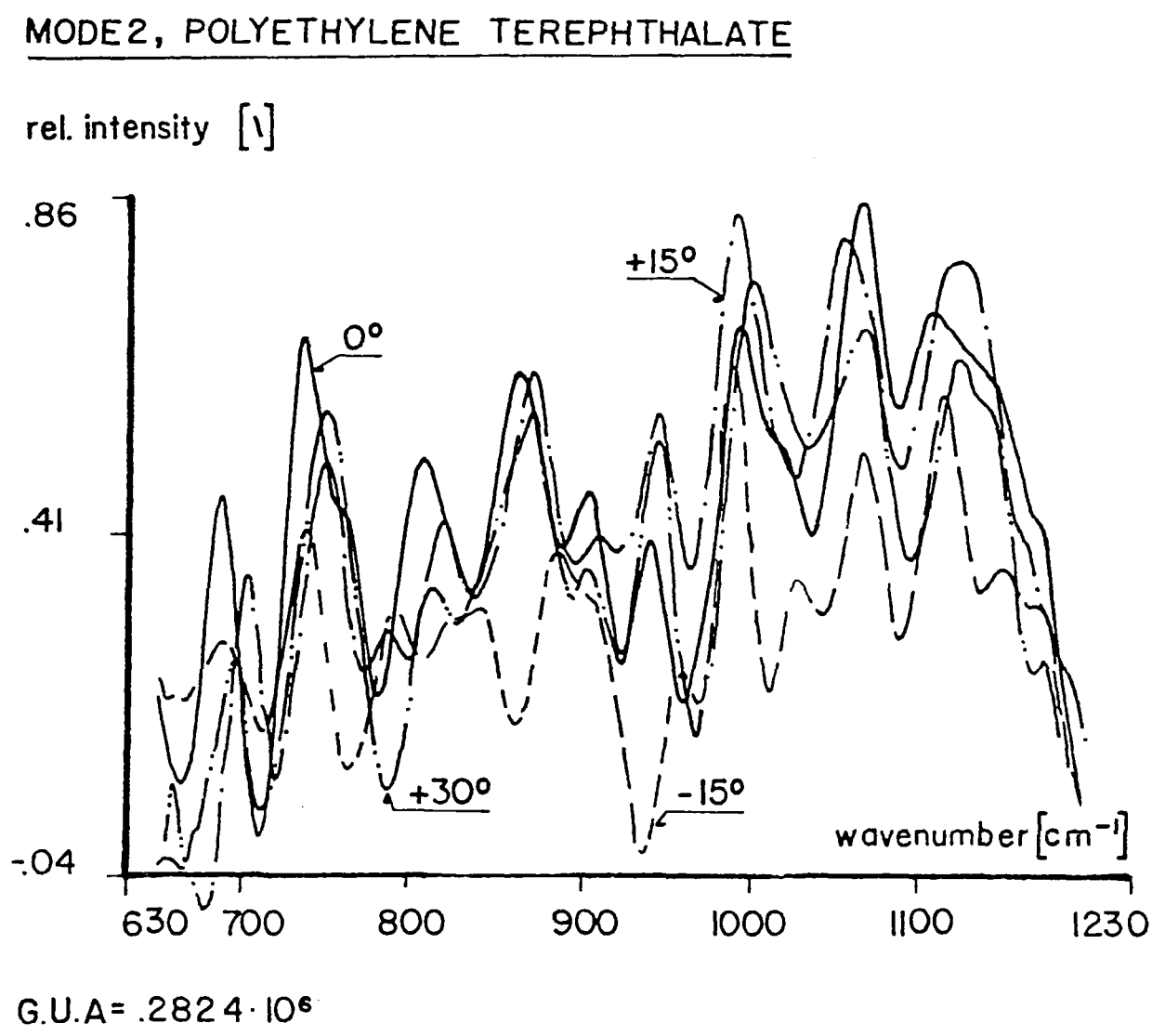

Figure 4.13 Series of polyethylene terephthalate spectra recorded in Mode 2

necessarily shown at their true frequencies. The sequences of the maximum relative intensity at all major bands for different phase angles are not identical, meaning that bands are oriented differently.

The maximum usable phase angle difference in Mode 2 operation, without changing the phase angle of the reference signal is limited. The signal received by the amplifier, i.e. the difference between the radiation parallel and perpendicular relative to the reference plane, will vanish if both directions radiate with the same intensity. Consequently, randomly oriented material cannot be analyzed in Mode 2. It is also possible that emission bands are displayed as absorption bands in Mode 2 operation, even with a perfectly isothermal sample. This effect is also due to the referencing procedure, and will occur if a strong band is oriented perpendicular to the plane of observation.

4.4.5 Mode 3 Operation

Polyethylene terephthalate was also used to verify Mode 3 Figure 4.14 shows the Mode 3 spectra, where the phase was varied in 15° steps over the whole period of 180°. In Figure 4.15 the intensities of three prominent bands are plotted as a function of phase angle. The local maxima identify the direction of a particular band. For nonoriented material the relative intensity is theoretically independent of the phase angle.

4.5 Other Apparatus Used in This Study

Although the apparatus used were already described elsewhere,

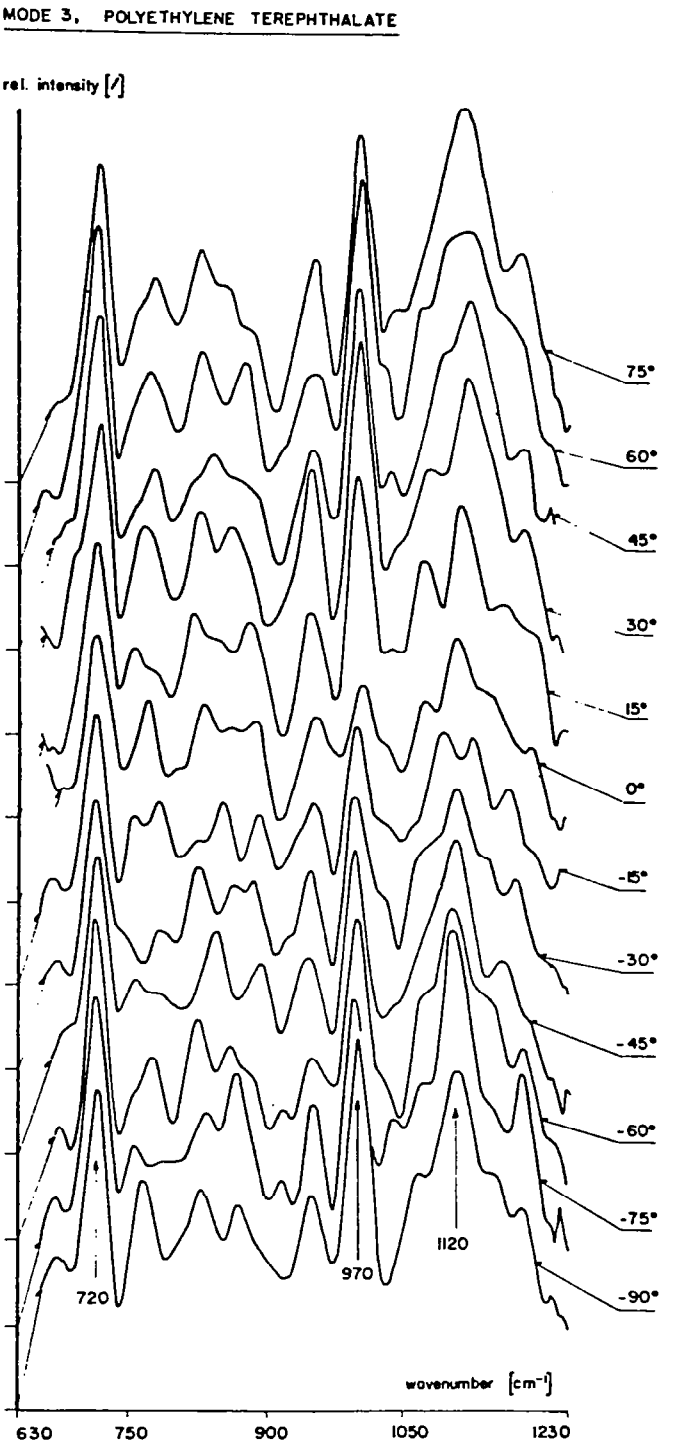

Figure 4.14 Series of polyethylene terephthalate spectra at different directions of the plane of polarization

MODE 3, POLYETHYLENE TEREPHTHALATE

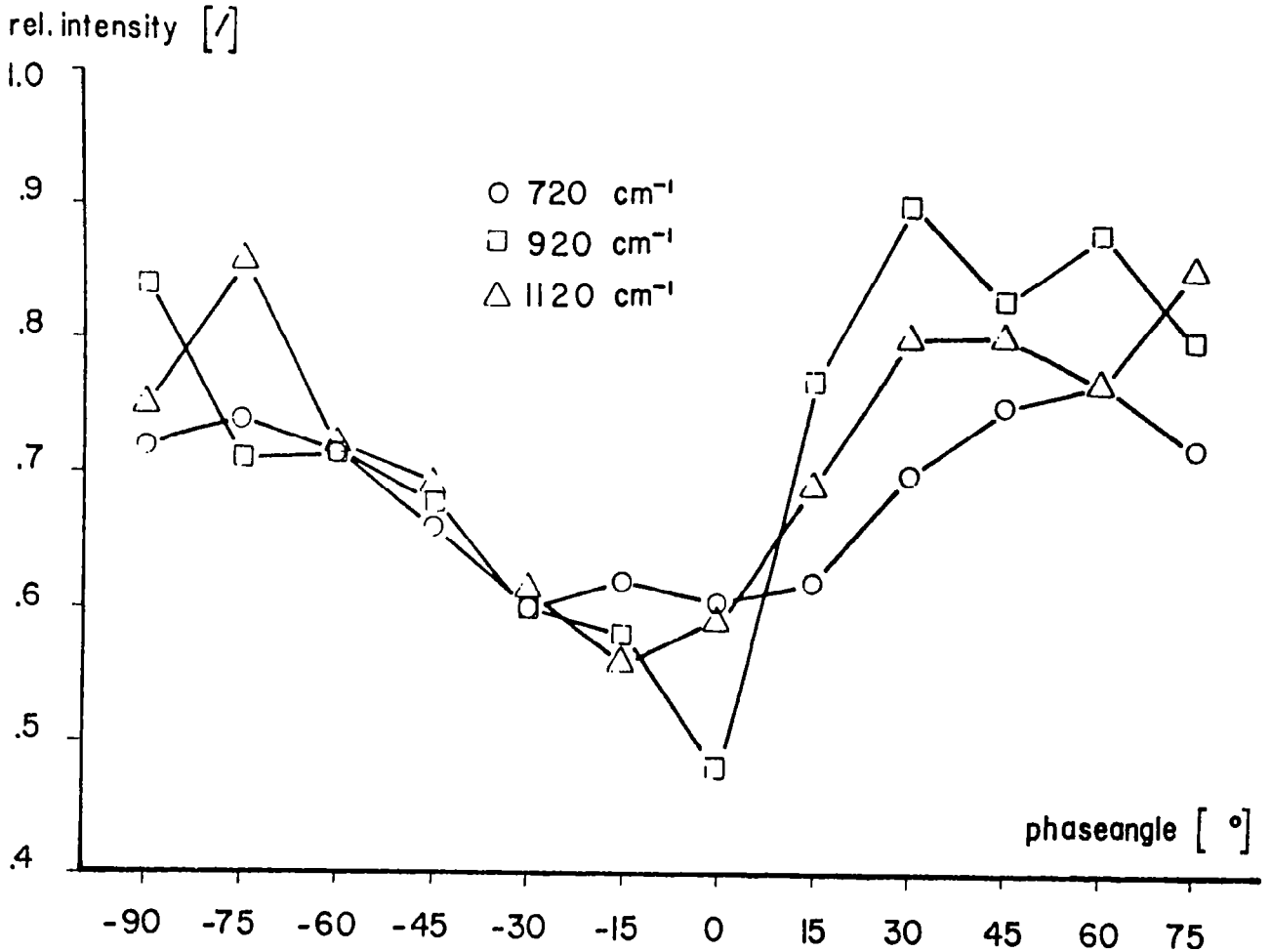

Figure 4.15 Intensities of three emission bands of polyethylene terephthalate as a function of the direction of the plane of polarization

an introduction to the sliding ball plate contact [2] and the measurement of film thickness and traction [3] is given.

4.5.1 Simulated Sliding EHD Ball Plate Contact

A 2 1/4" diameter ball is rotated in a cup, containing the test fluid, by an electric motor. Load is applied on the ball by a cantilever system. The ball is sliding on a 4 mm diameter and 2 mm thick diamond window, which allows the collection of infrared radiation in the Hertzian area from below the cup. Diamond was chosen for its high transparency at frequencies below 1800 cm^{-1}, its extreme hardness and its thermal conductivity. During operation the oil is heated rapidly by viscous friction. Cooling coils within the cup keep the system at constant temperature.

The temperature at the diamond window can be monitored by a thermocouple whose junction is attached to that window and buried in the mounting cement. Another thermocouple has its junction in a stagnant location of the cup to measure the average fluid temperature (T_B). The "diamond temperature" (T_D) measured with the thermocouple is very much lower than the true fluid temperature in the contact. Although the thermocouple is influenced by the surroundings, it is nevertheless a useful comparative measure.

4.5.2 Traction and Film Thickness Measurements

Traction and film thickness measurements relating to our sliding contact were obtained with the apparatus built by F. Choi [3] (Figure 4.16). It is similar to those described by Cameron,

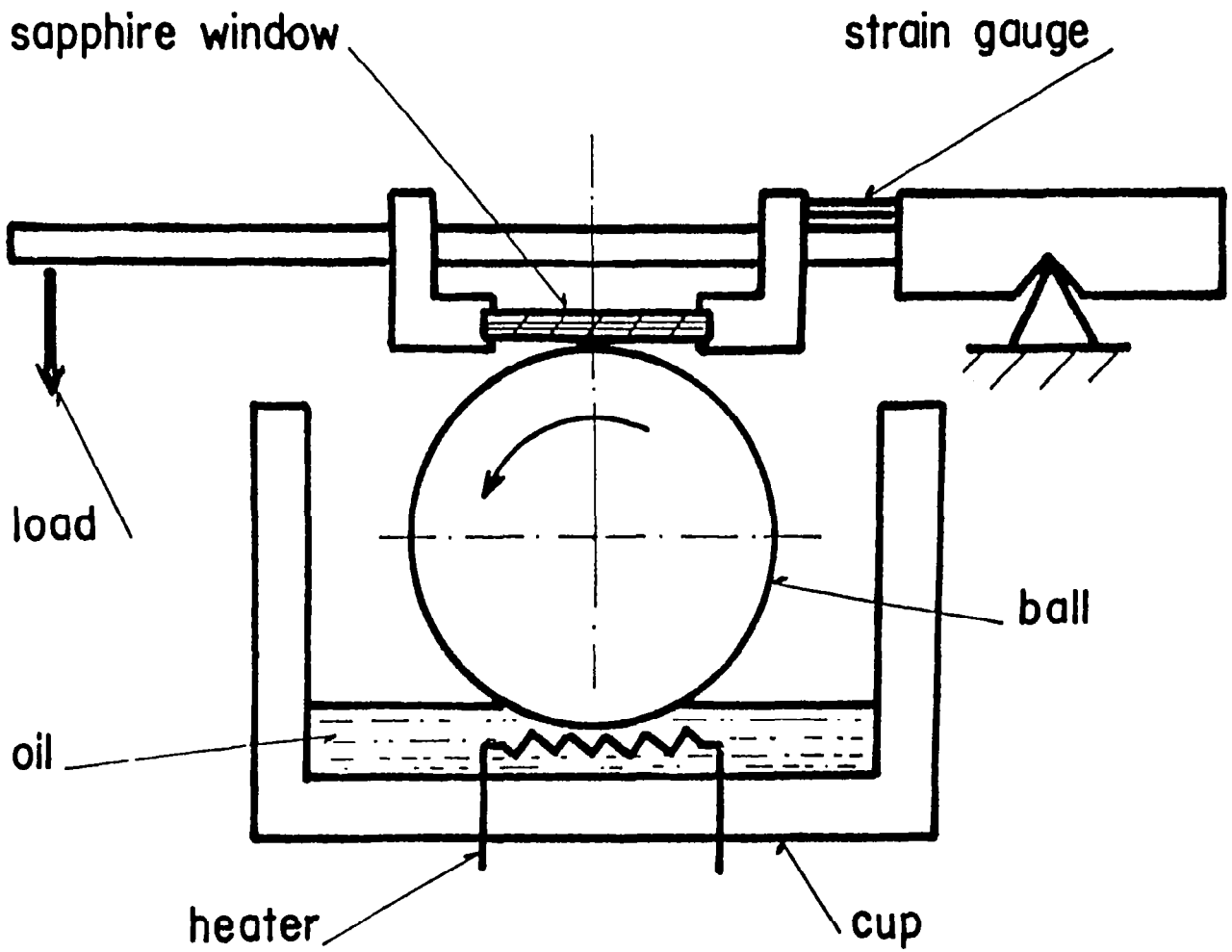

Figure 4.16 Apparatus for measuring traction and film thickness [3]

Winer and other authors. It consists of a rotating ball forming a sliding contact with a sapphire window on its upper surface, thus also allowing for convenient EHD film thickness measurements by microscopic observation of Newton rings. In our particular design, the sapphire window is 5 cm in diameter and 12 mm thick, both to allow easy access to the microscope objective and for heavily loaded contacts. The plate holding the window slides easily on linear bearings whose friction are insignificant compared to that of the EHD contact. The friction at the contact is determined with a strain gauge on the connection between the window plate and the loading platform.

4.6 Materials

The bearing balls were of 2.25" diameter and made of 440 C stainless steel. Some of them were coated with titanium-nitride (TiN) by chemical vapor deposition (CVD method) to a uniform thickness of about 4 μm by LSRH* [4]. The smoothness of the ball surfaces was about 0.01 μm (mean asperities height). Since the lubricant film thickness in the EHD contact under the heaviest load and at the smallest shear rate was at least 0.5 μm as shown later, direct asperity interaction was not anticipated to play a role.

All the experimental work concerning the simulated ball plate contact was carried out with polyphenyl ether. Poly-

*Laboratoire Suisse de Recherches Horlogeres, Neuchatel, Switzerland

phenyl ether, being solely aromatic and ether, provides excellent infrared spectra and is a rather pure chemical. It is still a mixture of many isomers, but many of the spectral bands can be assigned to the same transition moments. There are relatively few bands, many of them representing fundamental normal modes of vibration.

The additive used in many of the experiments was 1,1,2-trichloroethane separated from commercial trichloroethane by simple fractional distillation. Its infrared absorption spectrum showed no extraneous features. It has no strong bands of its own in the spectral region (630 - 1230cm^{-1}) of this investigation. Hence the spectra shown are not altered by its presence or absence, merely as a consequence of mixture. Its strong bands, strong enough to allow detection in concentrations of 1 percent or less, are below 600 cm^{-1}.

PART 5

RESULTS

5.1 Lubricants in an EHD Contact

5.1.1 Temperature Measurements

Table 5.1 lists the pertinent temperature measurements in the EHD contact under operating conditions when the system had been equilibrated. Two speed and load conditions are listed for both the TiN-coated and the uncoated balls for both neat and diluted (1% by volume of 1,1,2-trichloroethane, TCE) polyphenyl ether (5P4E). The following observations were noted:

For 5P4E without TCE, T_D is higher for the uncoated ball than for the TiN coated ball; the opposite is true for 5P4E with TCE. T_B is always lower for the uncoated ball than for the coated ball.

The temperature relations can be shown better when the increases ($\Delta T = T_D - T_B$) are compared in Table 5.2. All the ΔT's are higher for the uncoated ball than for the coated ball, but the differences made by the coating become smaller in the presence of TCE. With the uncoated ball, the presence of TCE causes a relatively large decrease of ΔT; the corresponding decrease with the coated ball is much smaller.

It should be pointed out that equilibrium conditions in the reservoir partly reflect the heat conducted away at the boundary surfaces of the EHD contact. The cooling coil around the contact in the cup removed the same amount of heat in every experiment since water from a large thermostated reservoir was pumped through. The bulk temperature T_B is especially sensitive to the overall thermal losses in the cup.

Table 5.1 EHD contact temperatures

SPEED	HERTZIAN PRESSURE	440C-BALL				TiN-BALL			
		NO ADD.		1% TCE		NO ADD.		1% TCE	
$[ms^{-1}]$	[GPa]	T_D [1]	T_B [2]	T_D	T_B	T_D	T_B	T_D	T_B
.6	.6	53.1	26.8	45.1	22.0	50.0	28.0	47.5	25.0
.6	1.2	63.4	27.2	54.9	23.5	58.5	29.3	54.9	26.2
1.2	.6	56.1	25.6	51.2	23.8	54.9	29.3	52.4	28.6
1.2	1.2	70.8	28.7	61.6	25.6	65.2	31.1	61.9	28.7

[1] T_D: DIAMOND TEMPERATURE IN [°C]

[2] T_B: BULK TEMPERATURE IN [°C]

Table 5.2 Temperature increases produced in the sliding EHD contact

SPEED [$m s^{-1}$]	HERTZIAN PRESSURE [GPa]	440 C-BALL		TiN-BALL	
		NO ADD.	1% TCE	NO ADD.	1% TCE
		ΔT [1]	ΔT	ΔT	ΔT
.6	.6	26.3	23.1	22.0	22.5
.6	1.2	36.2	31.4	29.2	28.7
1.2	.6	30.5	27.4	25.6	23.8
1.2	1.2	42.1	36.0	34.1	33.2

[1] ΔT: DIFFERENCE BETWEEN DIAMOND AND BULK TEMPERATURE IN [°C]

All the heat generated in the cup is generated in the lubricant sheared in the contact region and essentially all the heat losses are by conduction at the contact boundaries. It should be pointed out that the temperature measurements were simultaneous with and in the same apparatus as the spectroscopic measurements.

5.1.2 Traction and Film Thickness Measurements

The traction measurements were carried out under the same conditions as the spectroscopic and temperature measurements, but in the apparatus built specifically for this purpose. As a result, some difference must be expected for these reasons: (a) Instead of a diamond window constituting the plate of the ball/plate sliding contact, a sapphire window was used and (b) the ball/plate geometry was inverted with the ball below the plate in the traction apparatus. The main reason for these design differences was the space required for the microscope used in determining the lubricant film thickness optically; it is easier to look from the top down on a microscope than from the bottom up.

These differences should be only relative, however. The trends should be the same for the two setups. If we look at the traction results obtained for the intermediate load (Figure 5.1), the most outstanding difference is the high traction--ultimately leading to scuffing failure--for the stainless steel ball without the additive. The additive reduced the traction considerably in this case; scuffing still occurred, but at lower sliding speed. On the other hand, no scuffing ever occurred with the balls coated with titanium nitride. Here the influence of the chloride addition was very small, somewhat reducing traction at

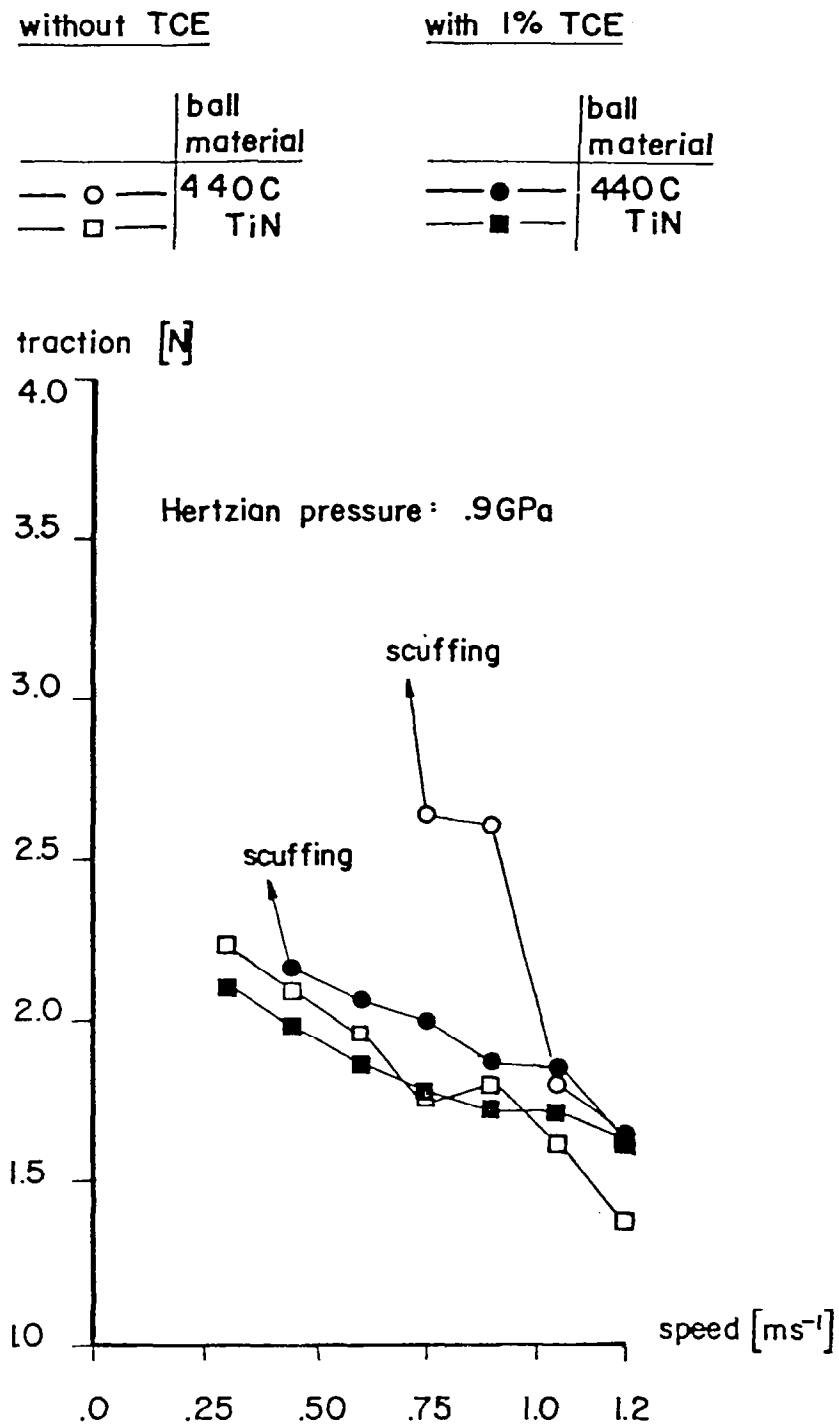

Figure 5.1 Force of traction from an EHD contact operating with polyphenyl ether (5P4E) with and without 1% 1,1,2-trichloroethane by volume

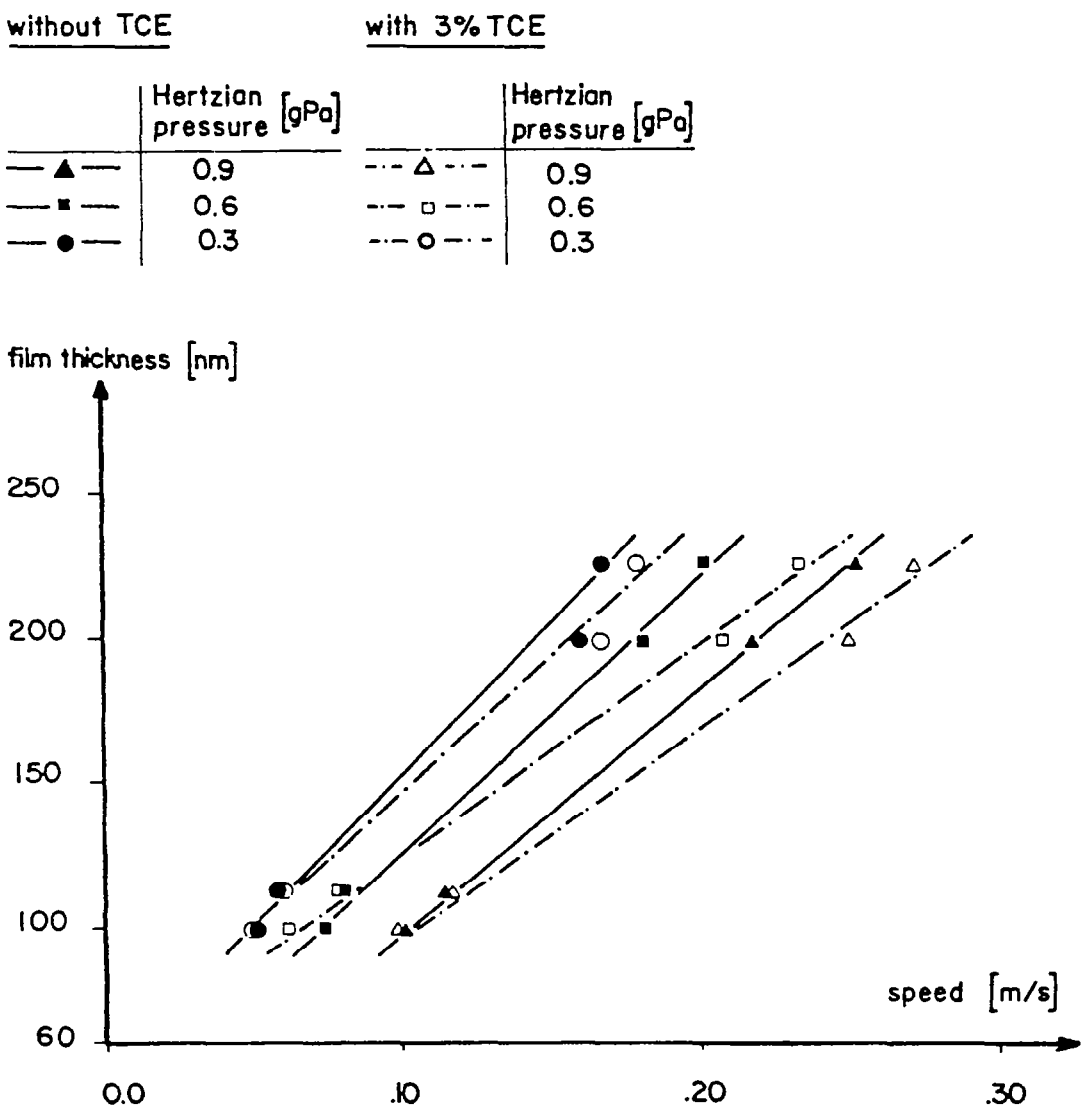

Figure 5.2 Hertzian contact separations obtained for a polycyclohexyl (traction) fluid with and without trichloroethane (TCE) additive at different average Hertzian pressures as a function of sliding speed.

low speed, but increasing it at high speed. The film thickness of polycyclohexyl (traction) fluid with and without TCE instead of polyphenyl ether was measured because of experimental limitations. The straight lines drawn in Figure 5.2 are the best curves fitting the data. The film thickness is smaller for the fluid with TCE than without for all loads at a given speed. Stability problems prohibited the data acquisition or lower speeds.

5.1.3 Infrared Spectra

Figure 5.3 shows a Mode 1 spectrum from a layer of stationary polyphenyl ether in the spectral region of interest. This spectrum is included here for reference. The relative intensities of the emission bands depend on temperature, pressure and polarization, so that they can be quite different for the emission spectra from the operating contact, but the frequencies (in cm^{-1} or wavenumber) should be essentially equal.

A very important factor in infrared emission spectroscopy is the constancy of temperature throughout the sample layer. A temperature gradient through the layer can cause reabsorption of some of the radiation emitted in warmer sublayers by colder sublayers and thus cause partial or total inversion of emission bands. In other words, emission bands can appear as absorption bands in an emission spectrum.

In Figure 5.4 unpolarized (Mode 1) spectra obtained under high speed/low load conditions from the contact are shown for the two different ball surfaces and the neat and TCE containing lubricant. The major emission bands at 870, 1110, and 1180 cm^{-1} stand out. The two bands

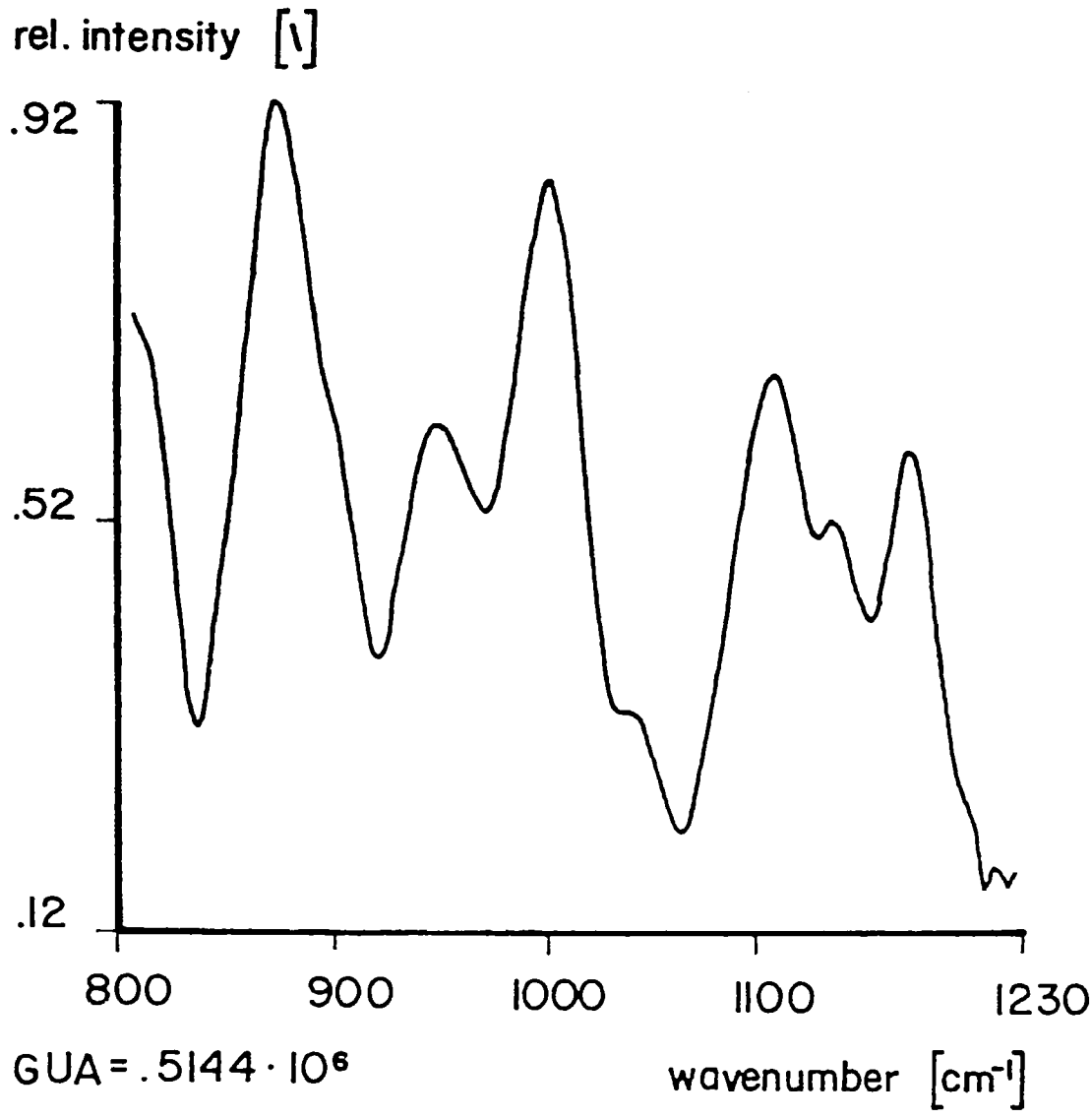

Figure 5.3 Static conditions infrared emission spectrum of polyphenyl ether (5P4E)

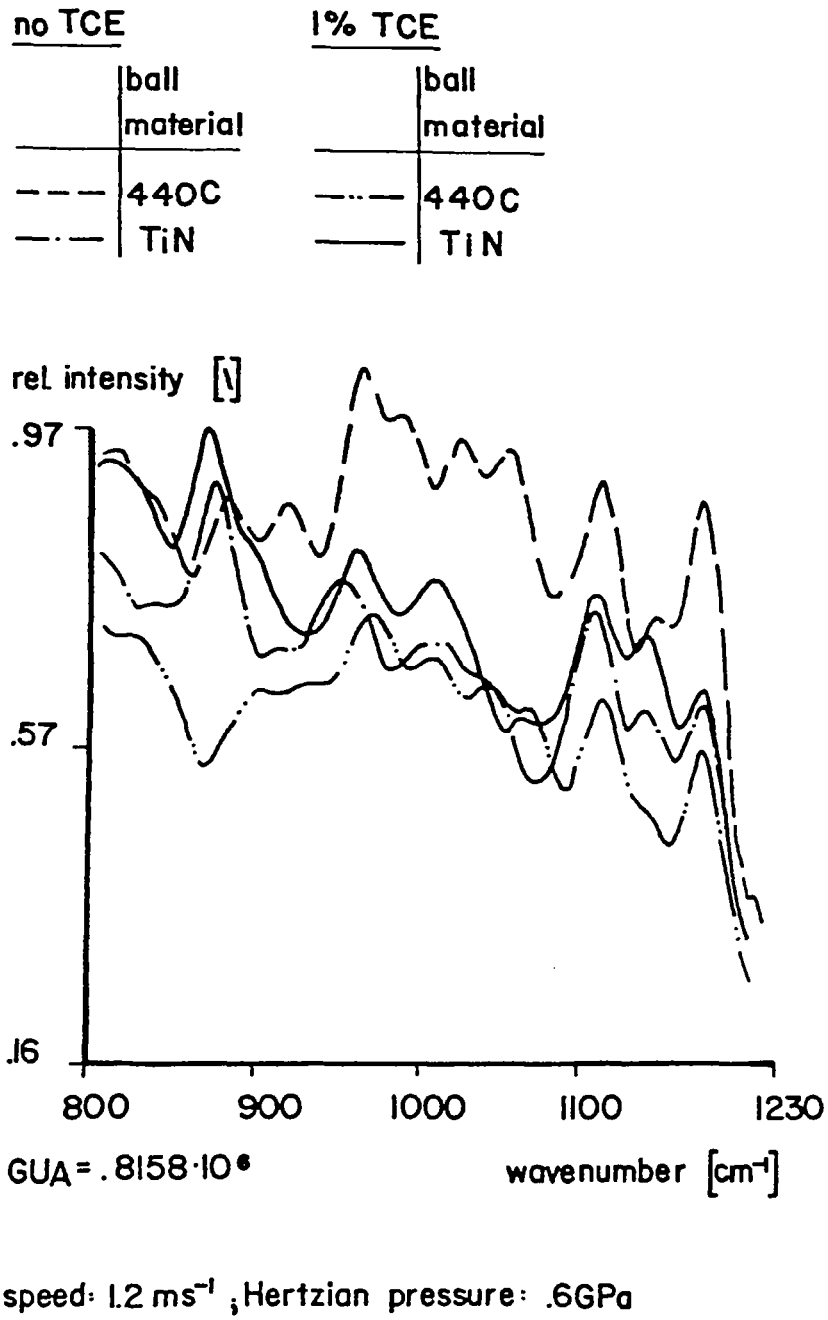

Figure 5.4 Comparison of Mode 1, i.e. unpolarized, emission spectra from an operating sliding EHD contact.

decrease in intensity in the order: steel/5P4E, coated steel/5P4E + TCE, coated steel/5P4E, and steel/5P4E + TCE. On the other hand, the 870 cm^{-1} band, which may experience a slight frequency shift due to experimental error, has the following order: coated steel/5P4E + TCE, coated steel/5P4E, steel/5P4E, and steel/5P4E + TCE. In the last case the band is fully inverted, indicating reabsorption. Some bands are more temperature-sensitive than others, so that reabsorption of one band does not imply reabsorption of all bands. A polarization related to molecular orientation can also come into play.

Comparison of the results for the 1110 and 1180 cm^{-1} bands with the entries in Line 3 of Table 5.1 for T_D shows excellent correspondence with the 1110 and 1180 cm^{-1} band intensities; conditions giving rise to the highest and lowest T_D's for example, also account for the highest and lowest band intensities. It should further be noted that these T_D's and band intensities refer to the uncoated steel ball and 5P4E without and with TCE. The unpolarized spectra corresponding to the entries of the other line of Table 5.1 show similar correspondence.

Polarized infrared emission spectra (Mode 3) obtained under the same load conditions as those of Figure 5.4 for the TiN-coated ball are plotted in Figure 5.5 to illustrate: (i) that the presence of TCE enhances polarization--intensity sequences and more definite, e.g. in the case of the 1110 cm^{-1} band--and (ii) that maximum and minimum intensities for most bands, but most clearly again for the 1110 cm^{-1} band, occur at 0° degree and 90° degree angles of the polarization plane with respect to the Hertzian conjunction plane (the Hertzian

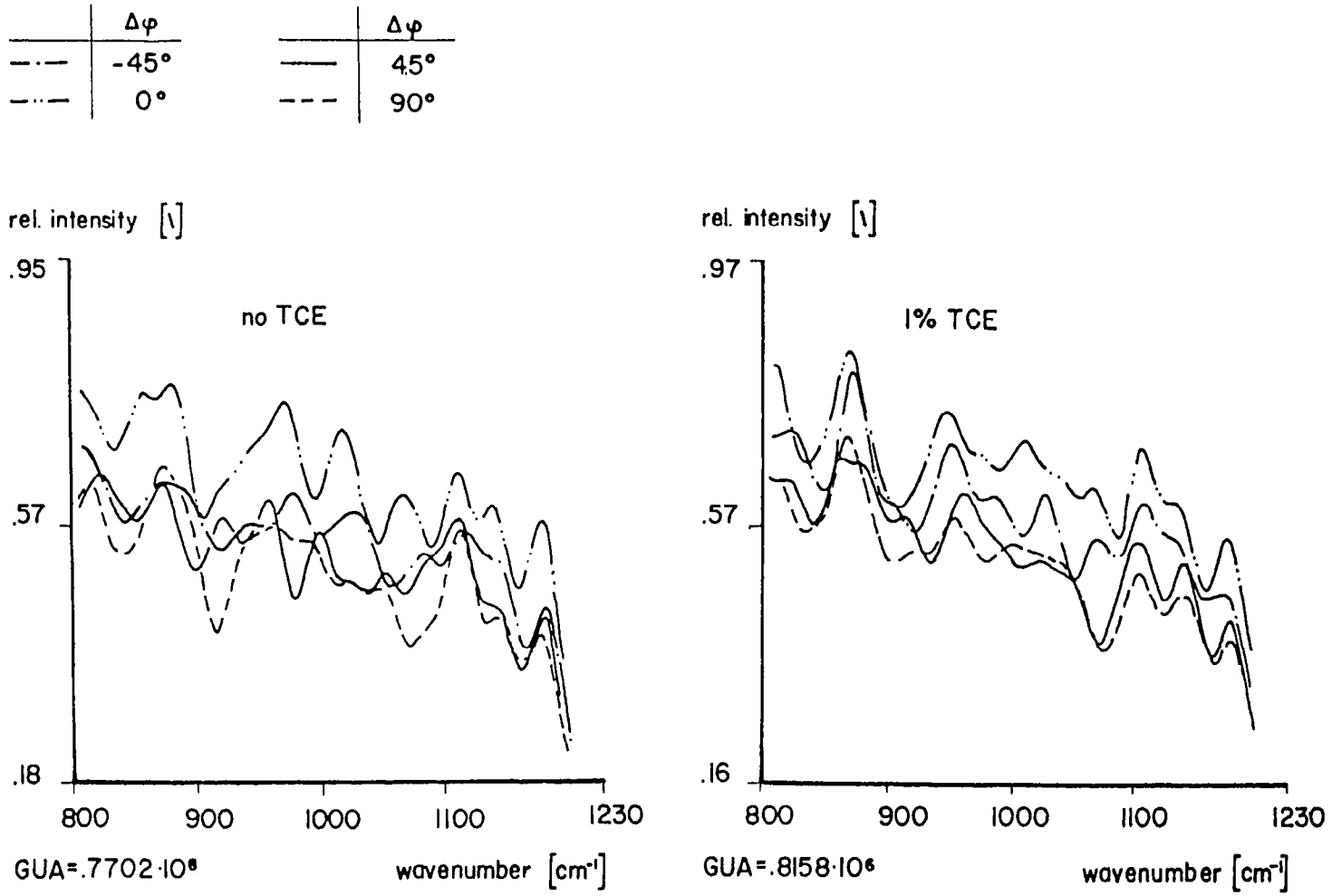

Figure 5.5 Mode 3 (polarized) spectra from an operating sliding EHD contact for the same condition as Figure 5.4

conjunction plane is defined as the plane containing the ball plate contact line and the center of the bearing ball).

Since it is often difficult to compare the spectra directly, the plots of Figure 5.6 were drawn from the data of Figure 5.7 for the 1110 cm^{-1} emission band intensities. Assuming the molecular dipole moment change vector corresponding to this band to be about aligned with the Hertzian conjunction plane, turning the polarization plane with respect to this plane by an angle ϕ should change the band intensity proportionally to $\cos^2\phi$ with half-period of 90° degrees. Since the alignment was not exact, the symmetry of the curves of Figure 7 is not perfect. The curves do show the increased amplitudes produced by the addition of TCE under all four pressure and speed conditions. Furthermore, to show the increased polarization even clearer, a quantitative measure P--simply the normalized standard deviation of the values plotted in Figure 5.6--is tabulated in Table 5.3 for the 1110 cm^{-1} band. Note that P is greatest for the highest load and speed and smaller for the smallest and that P is always greater when TCE is present than when it is absent. The reason for the different order of the intermediate P values with and without TCE is not clear.

That the curves plotted in Figure 5.6 do not parallel a $\cos^2\phi$ wave can be deduced from inequality of the intensities for +45° and -45° for each of the four curves. Interestingly +45° and -45° intensities are more closely the same when TCE was absent than present. Mode 2 spectra automatically yield the difference between band intensities in polarization planes whose angles with the reference plane differ by 90°. For example, if a plane at 45° from the Hertzian conjunction

Table 5.3 Relative spectral polarization as a function of the operating conditions of the EHD contact with the TiN-coated ball

SPEED [ms^{-1}]	HERTZIAN PRESSURE [GPa]	POLARIZATION P NO ADD. [1]	POLARIZATION P 1% TCE [1]
.6	.6	.48	.68
.6	1.2	.63	.80
1.2	.6	.41	.84
1.2	1.2	.91	1.00

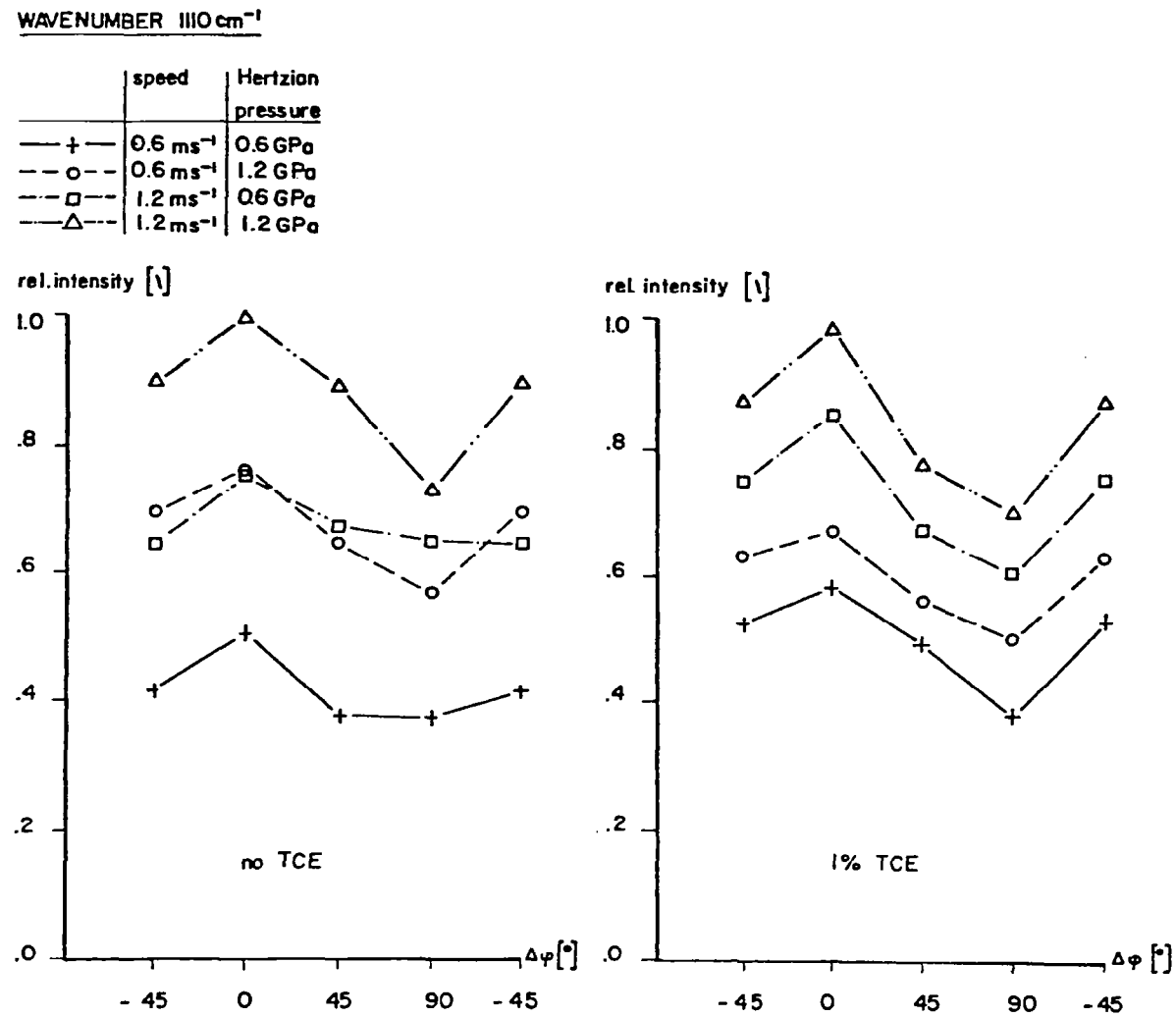

Figure 5.6 Variation of the intensity of the 1110 cm^{-1} infrared emission band of 5P4E polyphenyl ether with and without 1% of trichloroethane as a function of polarizer orientation for different speeds and pressures. The data were obtained from the Mode 3 spectra with the TiN-coated ball

plane, i.e. $\phi = 45°$, were the reference plane, then Mode 2 spectra would give the differences between the values of the intensities shown for +45° and -45° in Figure 5.6. These differences would not be zero for the case of TCE present, but close to zero for TCE absent. Thus it would seem that TCE not only increases the degree of polarization P and thus the molecular alignment in the EHD contact but also the direction of the transition moment corresponding to the 1110 cm^{-1} band as well. In other words, while the projection of this moment in the plane of the polarizer would seem to be coincident with the Hertzian conjunction plane, $\phi = 0$, for the highest speed and load when TCE is absent--for then the relative band intensities at $\phi = +45$ and $\phi = -45°$ are equal--it is inclined to this plane when TCE is present.

To pursue this idea further the Mode 2 data of Figure 5.7 were plotted for the 1180 cm^{-1} band from spectra obtained with a TiN-coated ball under the four operating conditions of 5P4E both without and with 1% of TCE by volume. It will be noted that the relative band intensities at $\Delta\phi = -30°$, corresponding to $\phi = -30°$ and +60° with the conjunction plane are minimal and about equal for all conditions with TCE present. This would mean that the projection of the transition moment vector giving rise to this infrared band is making an angle $\phi = +15°$ with the Hertzian conjunction plane. Clearly the direction of the transition moment is different when TCE is absent. Due to initial problems with the angular calibration of the polarizer, the direct comparison of the phase angles indicated in Figures 5.7 and 5.8 is not possible. Both show Mode 2 data of the relative intensity at 1180 cm^{-1}. The results of Figure 5.8 were obtained with the steel ball. With TCE

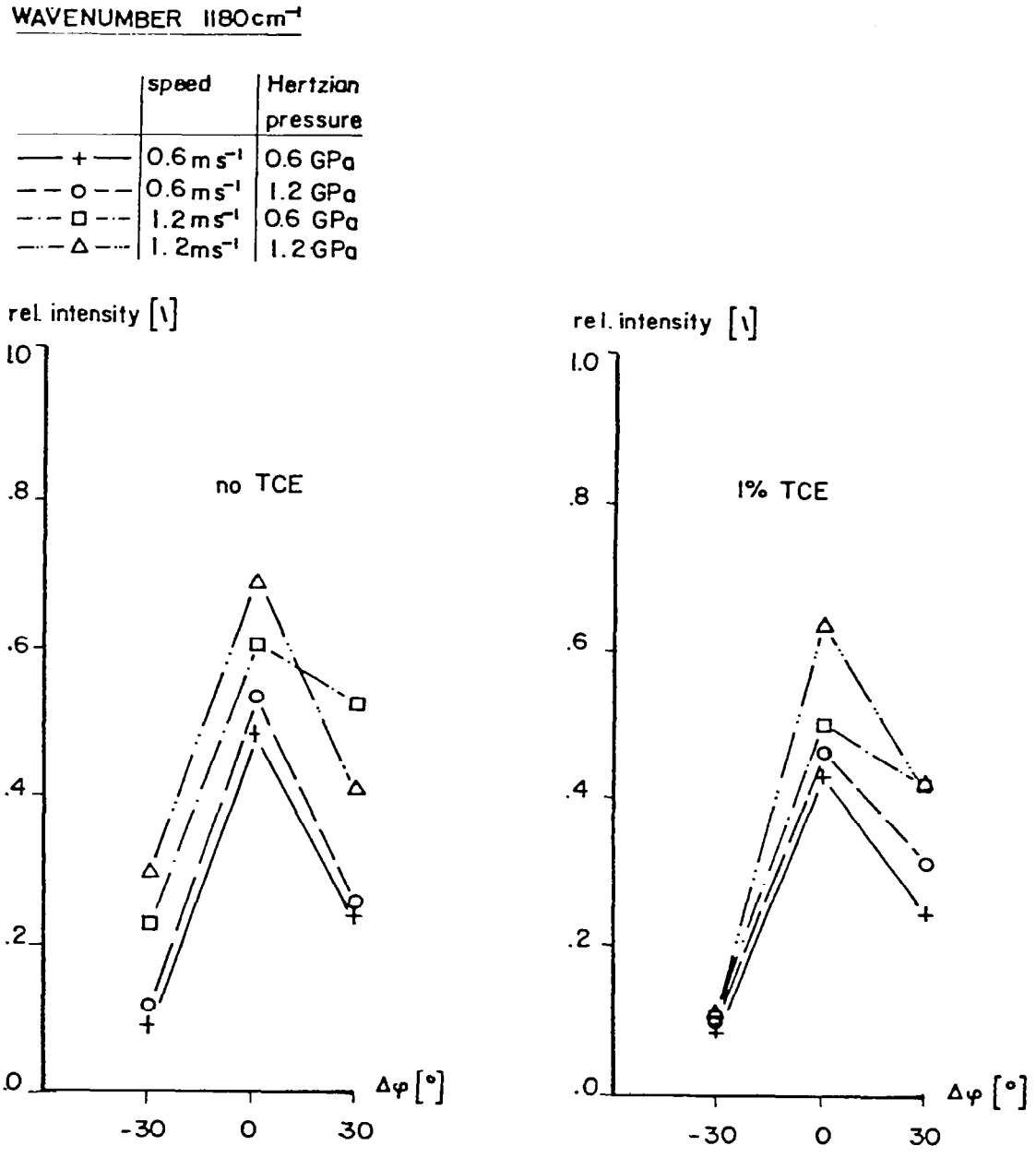

Figure 5.7 Intensity differences of the 1180 cm^{-1} band determined for mutually perpendicular polarizer orientations with change of reference position. The spectra were obtained with a TiN-coated ball and with polyphenyl ether fluid with and without 1% of trichloroethane

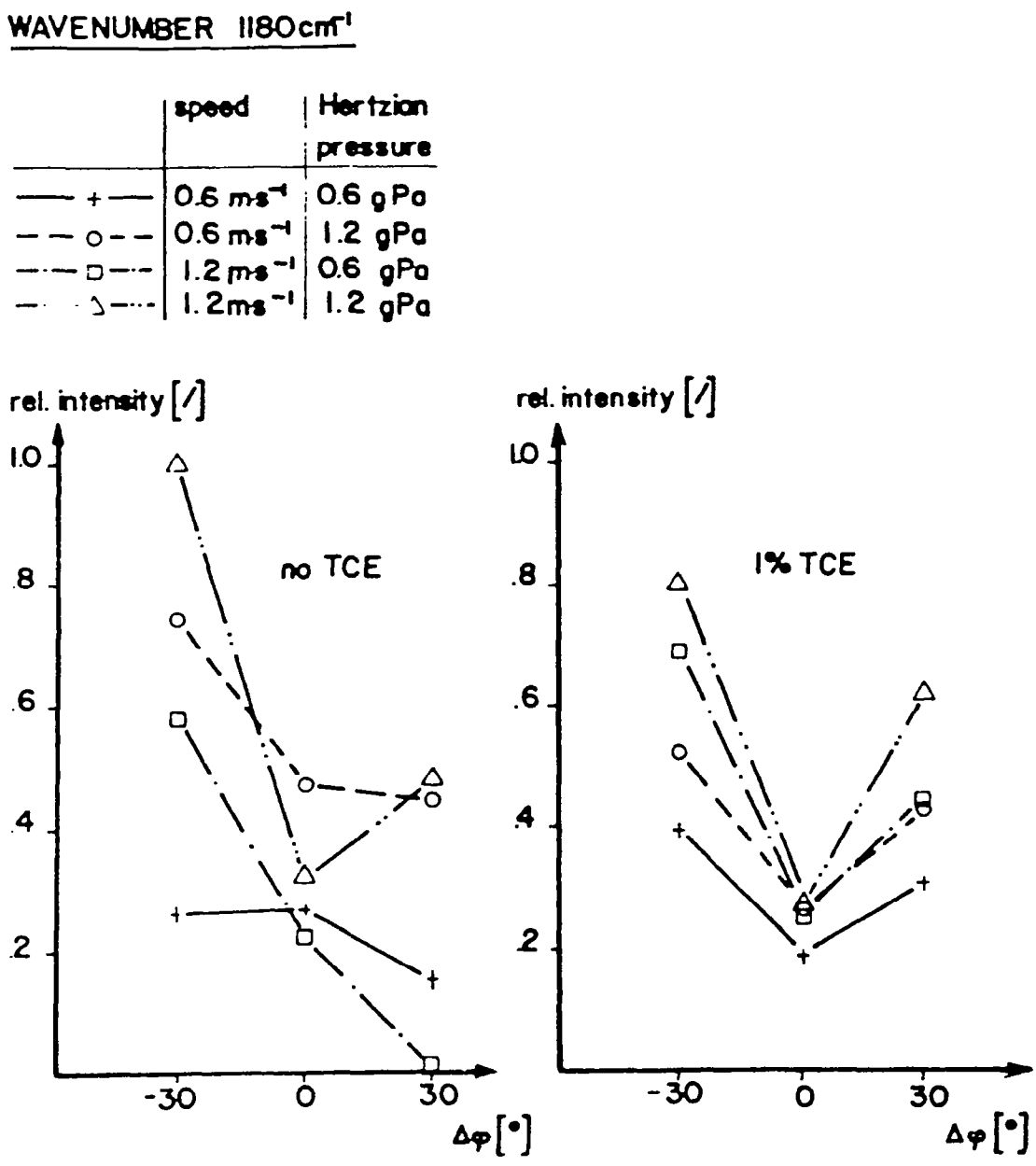

Figure 5.8 Intensity differences of the 1180 cm^{-1} band determined for mutually perpendicular polarizer orientations with change of reference position. The spectra were obtained with a 440 C ball and with polyphenyl ether fluid with without 1% of trichloroethane

present, a regular pattern for all loads and speeds is shown. Without TCE, the "V" type pattern is only recognizable at highest load and speed. Both of these bands represent in-plane bending vibrations of the aromatic ring of 5P4E; the corresponding transition moments should therefore cause radiation to propagate into the interferometer when the rings are aligned parallel to the diamond window. None of the specific TCE infrared bands are expected to show in the emission spectra of this frequency region.

5.1.4 Measurement of Phase Changes

Figure 5.9 shows glass transitions for the polycylcohexyl (traction) fluid and for a 1 percent solution of TCE in it, which were obtained by differential thermal analysis (DTA). The assumption of a correspondence of temperature decrease with pressure increase is commonly made. The change in slope of the heat capacity/temperature/plots indicate glass transitions. The absolute values of the transitions are less important to us here than the fact that the presence of TCE produced a second glass transition, even though the solution at room temperature was perfectly clear. Somewhere along the line, a phase separation occurred on cooling. When a similar solution was pressurized to very high pressure (up to 12 kbar) in a diamond anvil cell, phase separation (a spider net pattern) was observed suddenly under the phase contrast (polarization) microscope. While these experiments were conducted under low shear--or no shear--conditions, there is every reason to believe that the same phenomenon would occur under shear and, theoretically, would be even more drastic. In other words, it is very likely that the lauric

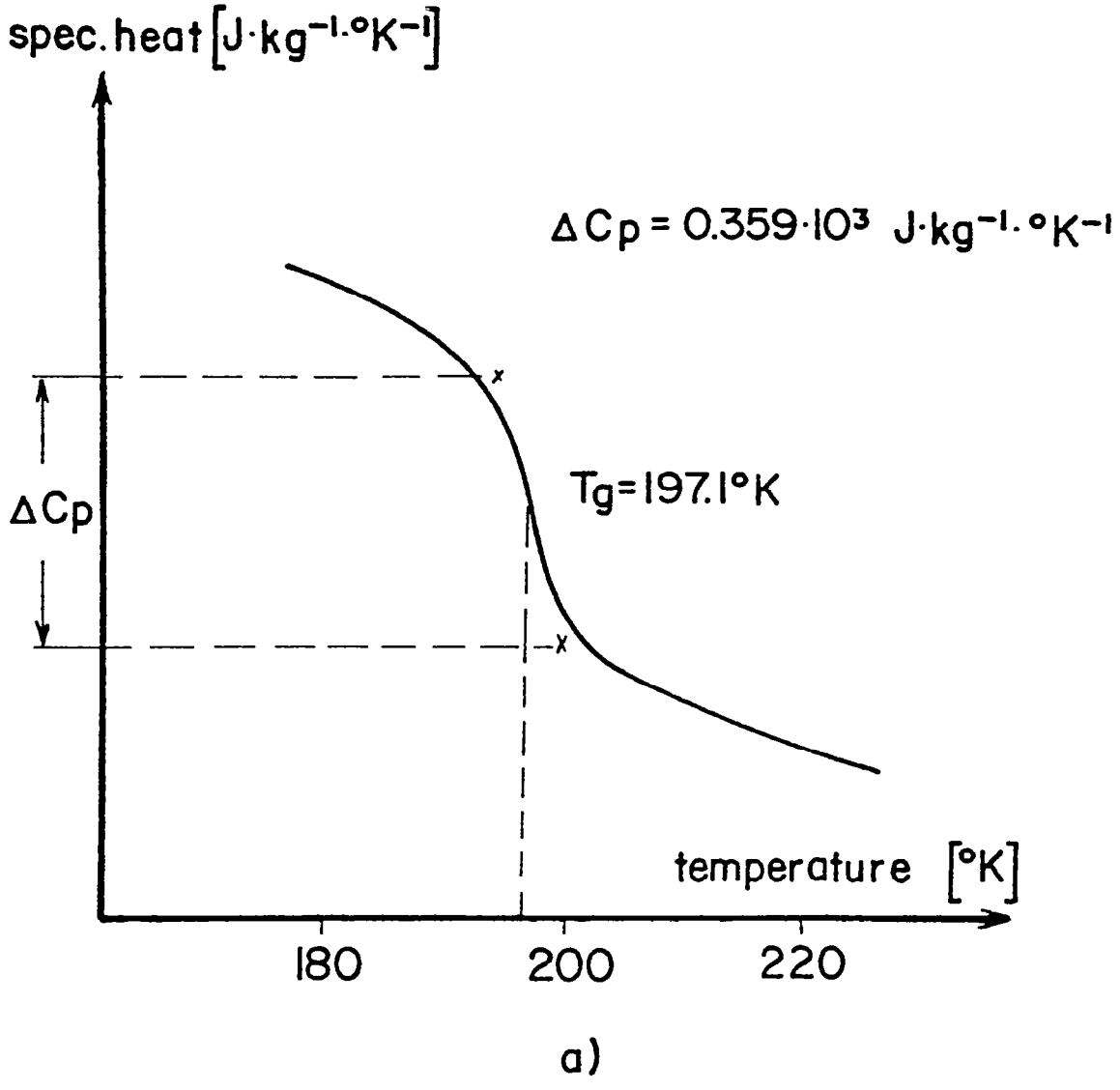

Figure 5.9a Differential thermal analysis (DTA) of polycyclohexyl (traction) fluid

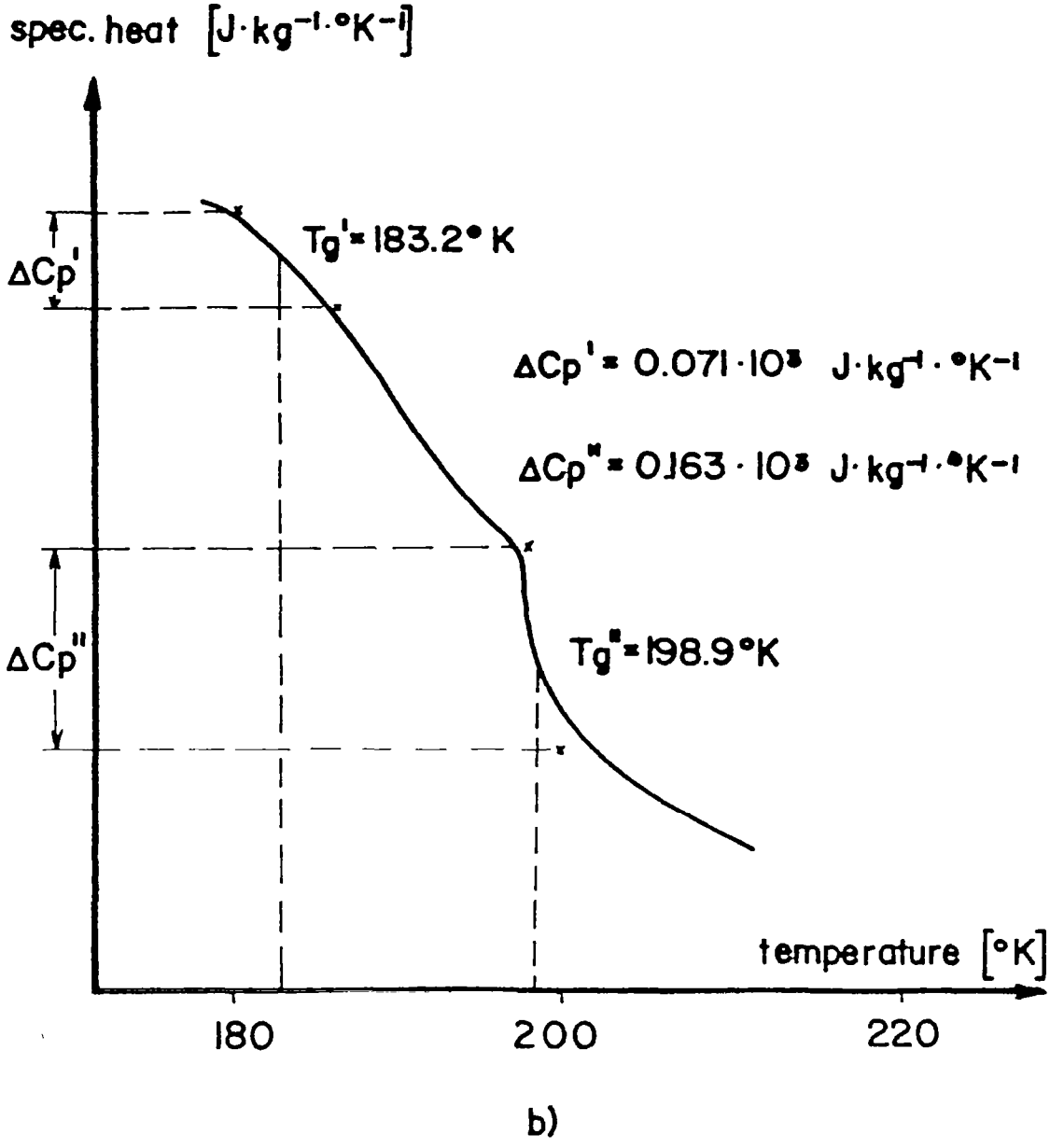

Figure 5.9b Differential thermal analysis (DTA) of polycylohexyl (traction) fluid with 3% of trichloroethane

acid and other commonly used boundary additives--help produce a two-phase or multi-phase system (liquid/liquid or liquid/solid) under Hertzian contact pressures.

5.2 Aircraft Fuel Line Deposits

5.2.1 Infrared Spectra of Actual Fuel Lines

Preliminary measurements were done with actual fuel lines. The purpose of this study was to show a sufficient spectral contrast for chemical analysis and to prove that the deposits are oriented.

For these measurements the samples were cut open and pressed flat. In most cases the deposit did not flake off. Figures 5.10, 5.11 and 5.12 illustrate the effect of orientation combined with the power of Mode 2. The Mode 2 spectra vary significantly with phase angle which, in a general way, corresponds to the direction of the temperature gradient responsible for the deposition of the "coke". The Mode 1 spectra show the most significant bands. Figures 5.13, 5.14 and 5.15 contain plots of the intensities of two of these bands against phase angle, using Mode 2 data. Clearly the 720 cm^{-1} band data are displaced with respect to the 1020 cm^{-1} data, indicating molecular alignment and different orientation of the corresponding transition moments.

5.2.2 Infrared Spectra of Test Specimens

In an apparatus specially built and operated by NASA, deposits on steel strips, forming part of a simulated fuel line, were obtained. Nitrogen contents and the temperature of any fuel passing through the thermal stability simulator can be adjusted. The samples shown in

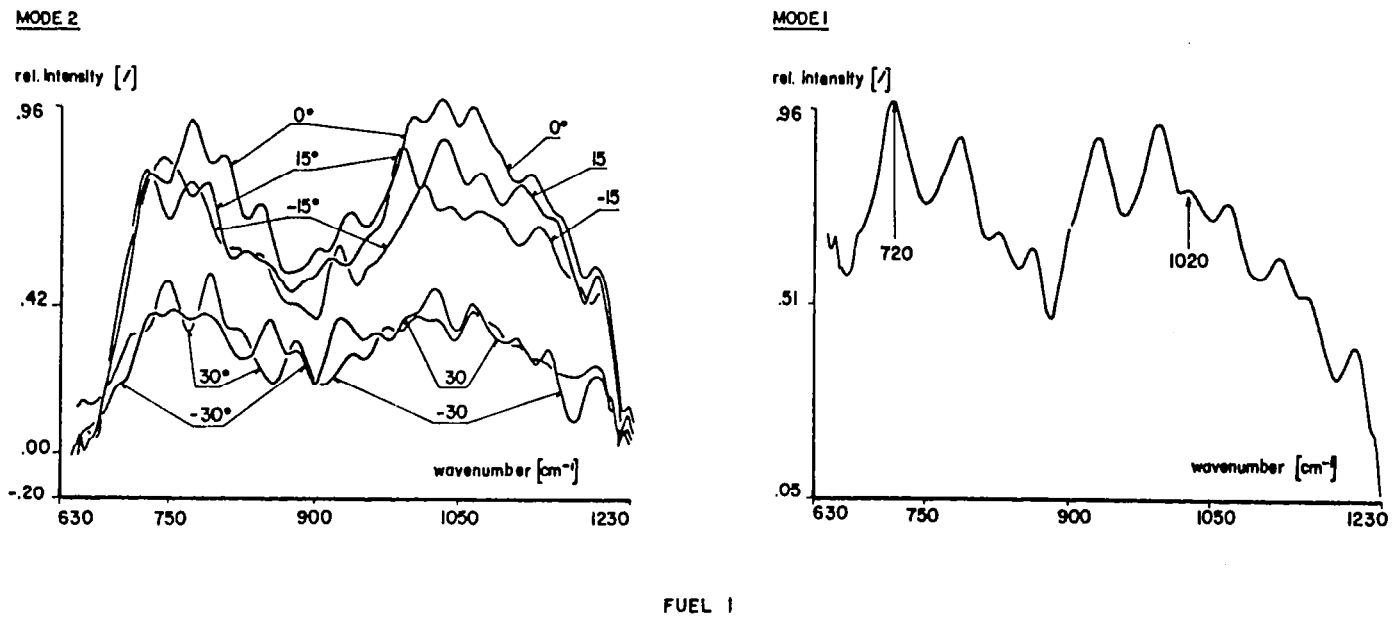

Figure 5.10 Emission spectra of an aircraft fuel line deposit (Fuel 1) obtained by Mode 1 and Mode 2

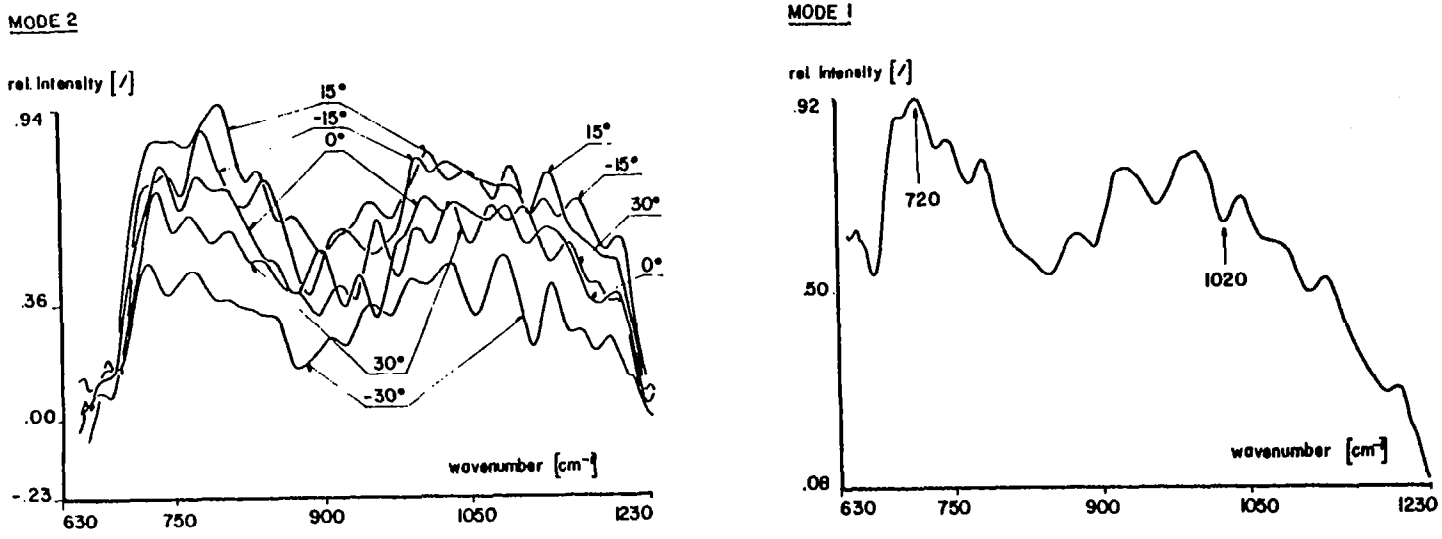

Figure 5.11 Emission spectra of an aircraft fuel line deposit (Fuel 2) obtained by Mode 1 and Mode 2

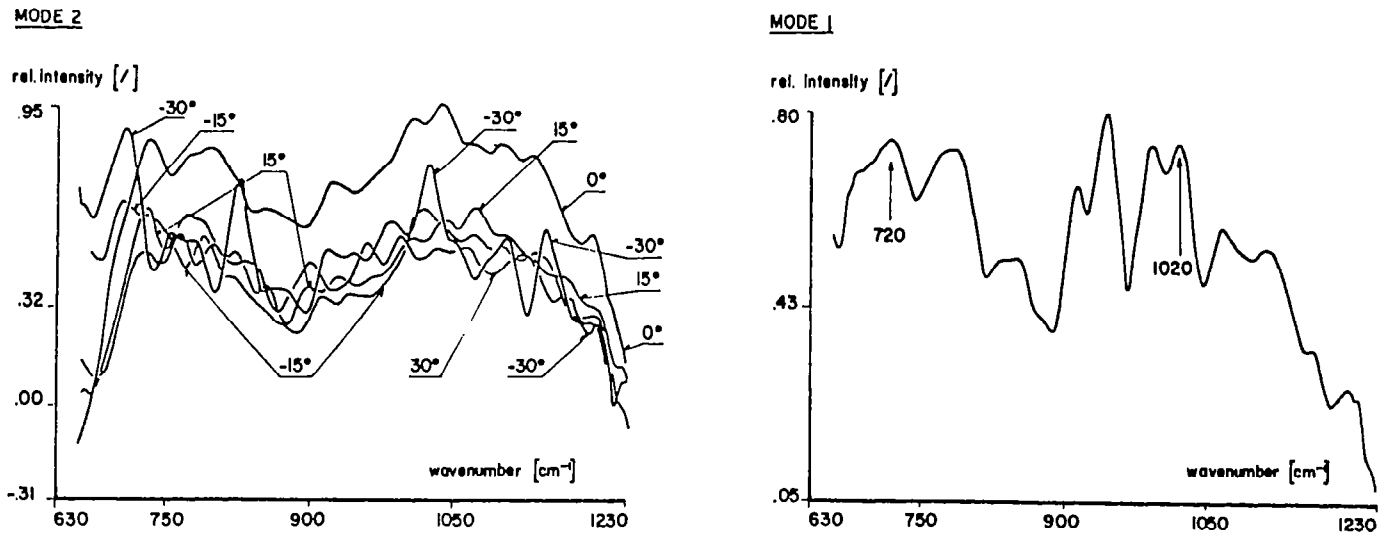

Figure 5.12 Emission spectra of an aircraft fuel line deposit (Fuel 3) obtained by Mode 1 and Mode 2

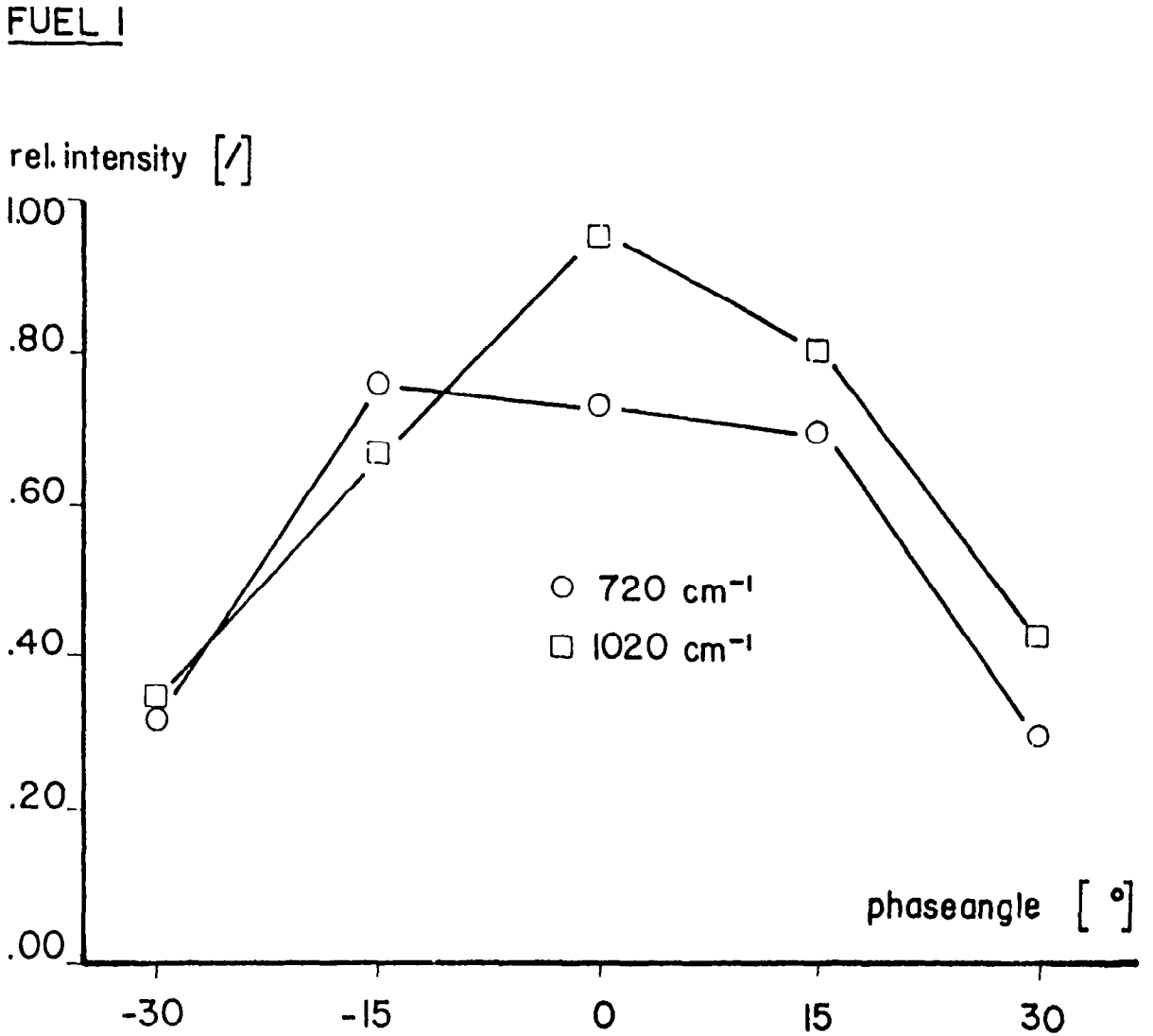

Figure 5.13 Change of two band intensities with phase angle for Fuel 1 (compare Figure 5.10)

FUEL 2

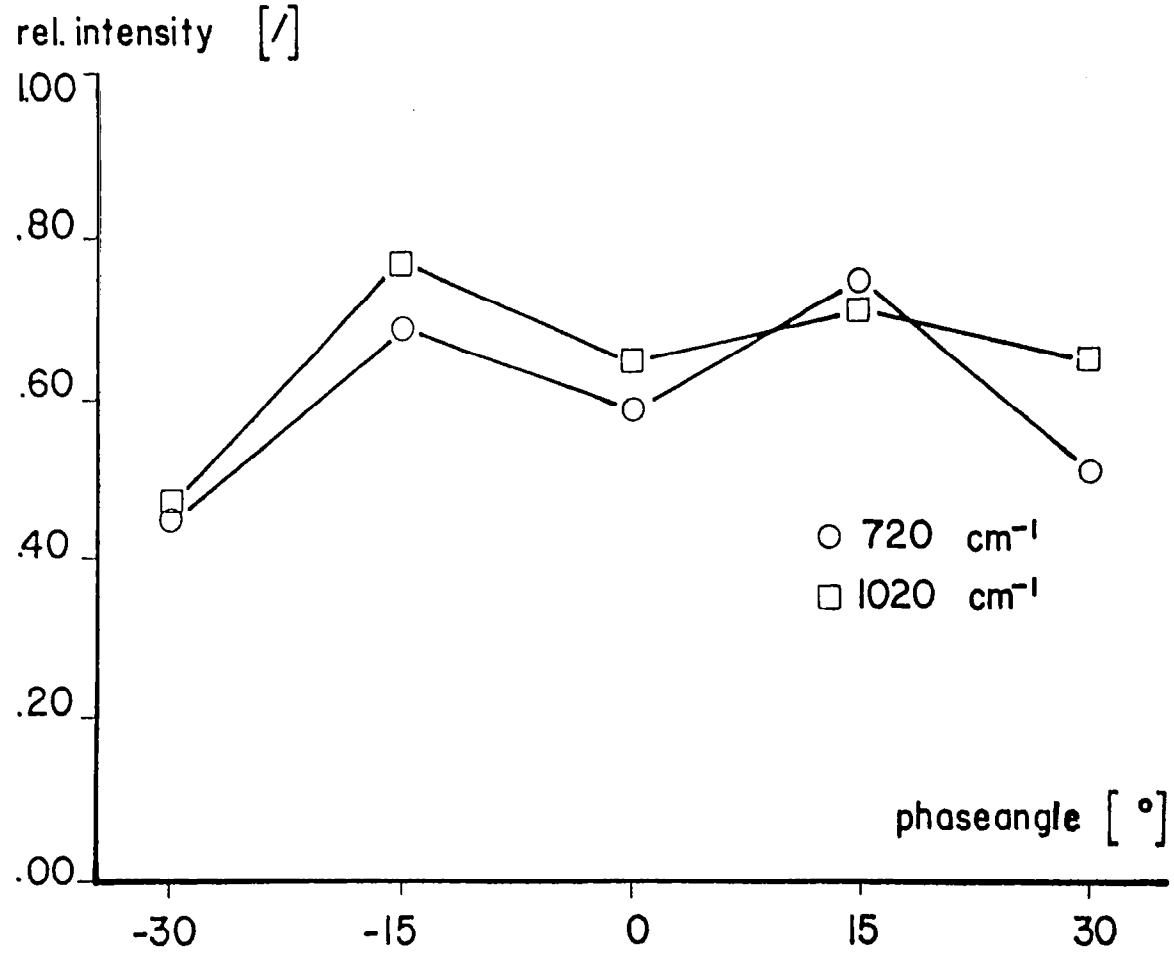

Figure 5.14 Change of two band intensities with phase angle for Fuel 2 (compare Figure 5.11)

FUEL 3

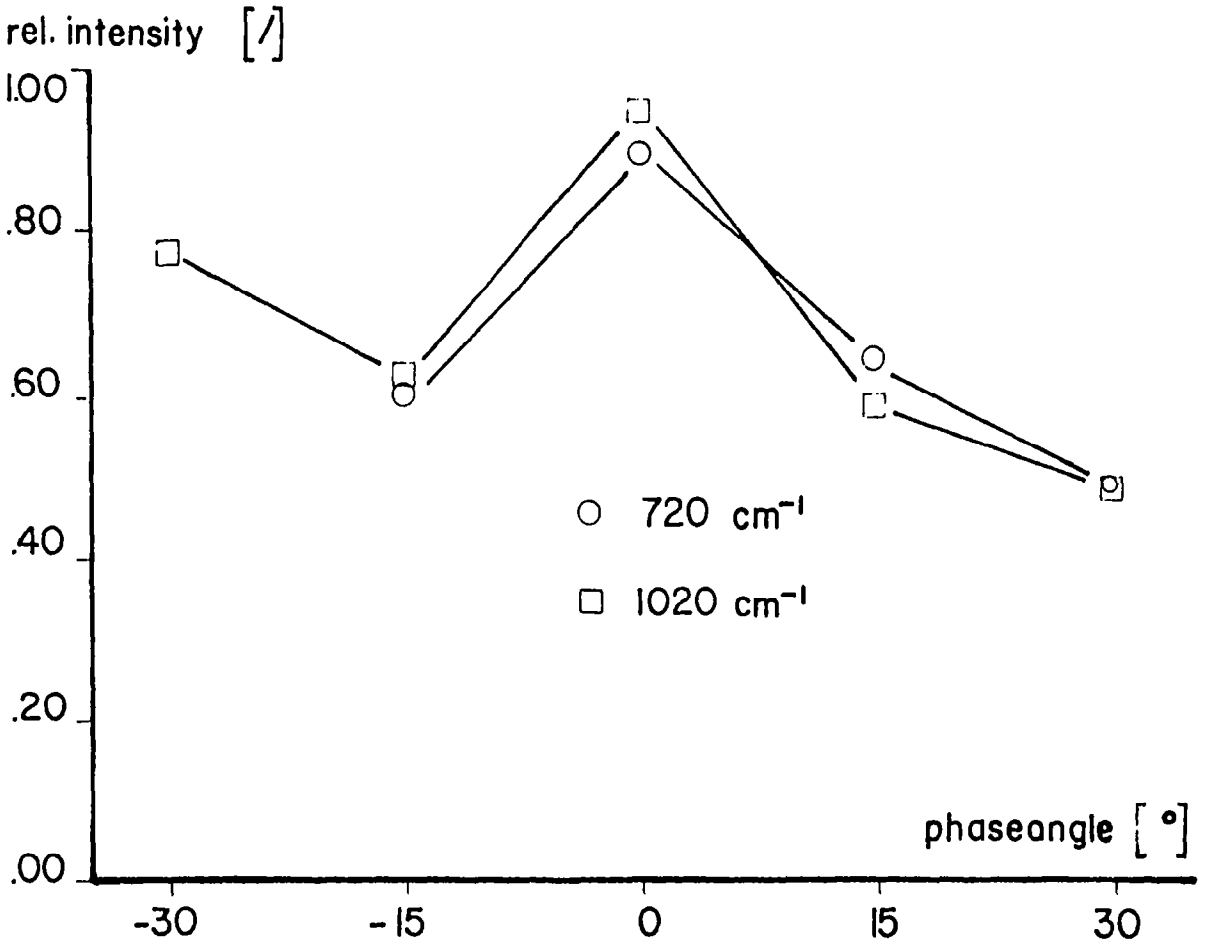

Figure 5.15 Change of two band intensities with phase angel for Fuel 3 (compare Fig. 5.12)

Table 5.1 were analyzed in all three modes between 630 and 1800 cm^{-1}. Figure 5.16 shows the spectrum of the sample with the lightest coating. Mode 1 and Mode 3 data were plotted on the same graph, despite the different aperture settings. Mode 3 Spectra are helpful, primarily in identifying weak spectral features, which are not resolved in the Mode 1 data.

An in-depth analysis of the chemical composition of the deposits was not done in this report. The principal method of chemical analysis is to evaluate the position and strength of emission bands, as shown in Figure 5.16. Charts, as published in [21] allow the identification of the deposits.

5.2.3 Accelerated Oxidation

Sample #15 (Table 5.4) was produced under nearly the same condition as #49 but 1 year earlier. After its spectral analysis, sample #49 was subjected to accelerated oxidation by heating to 150°C in a stream of air for one hour and then run again.

Figure 5.17 gives a comparison of the spectra of all the samples received with the spectrum of the oxidized sample. Note in particular the broad structures peaking near 720, 820, and 880 cm^{-1} and the 1010/1035 cm^{-1} doublet. All these structures seem to contain both the original bands of these regions, which are displayed by the unoxidized #49 spectrum plus one other band of #50, which was slightly displaced toward lower frequencies. Thus the 720 cm^{-1} structure contains both bands of #49 and #50 doublets (which are similar in this region), but with the lower frequency partner (710 cm^{-1}) strengthened; the 820 cm^{-1} structure has a shoulder at 800 cm^{-1} corresponding the #50 band at this position, the 880 cm^{-1} doublet consists of a band at 880 cm^{-1},

Table 5.4 Summary of deposits on shims

#	Weight	Date	Temperature	Run Time
14	16.0 μg	7/ 7/80	475°F	150.0 min
49	6.9 μg	7/21/81	485° F	150.7 min
50	7.8 μg	7/21/81	487° F	150.4 min

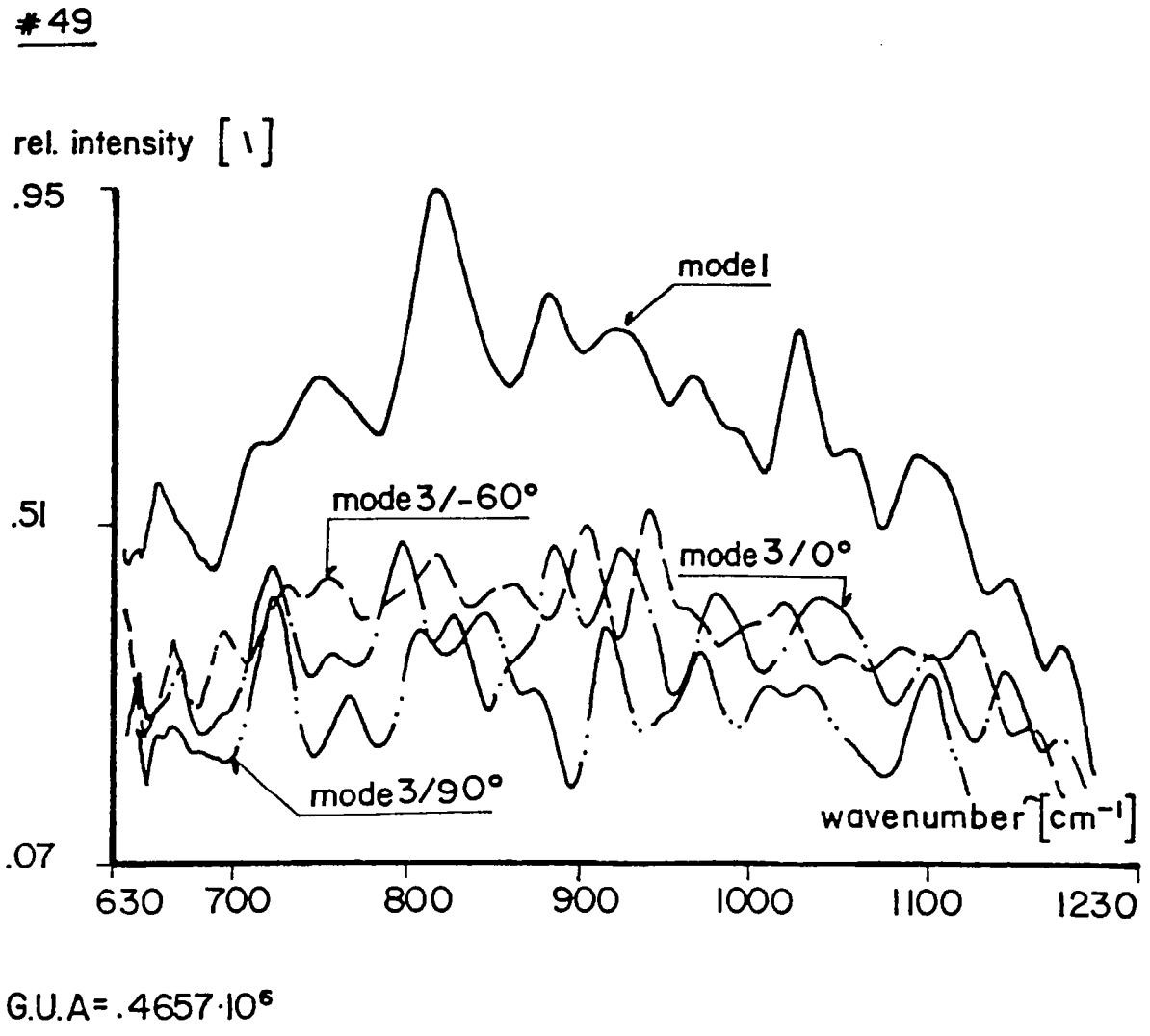

Figure 5.16 Comparison of Mode 1 and Mode 3 spectra of sample #49

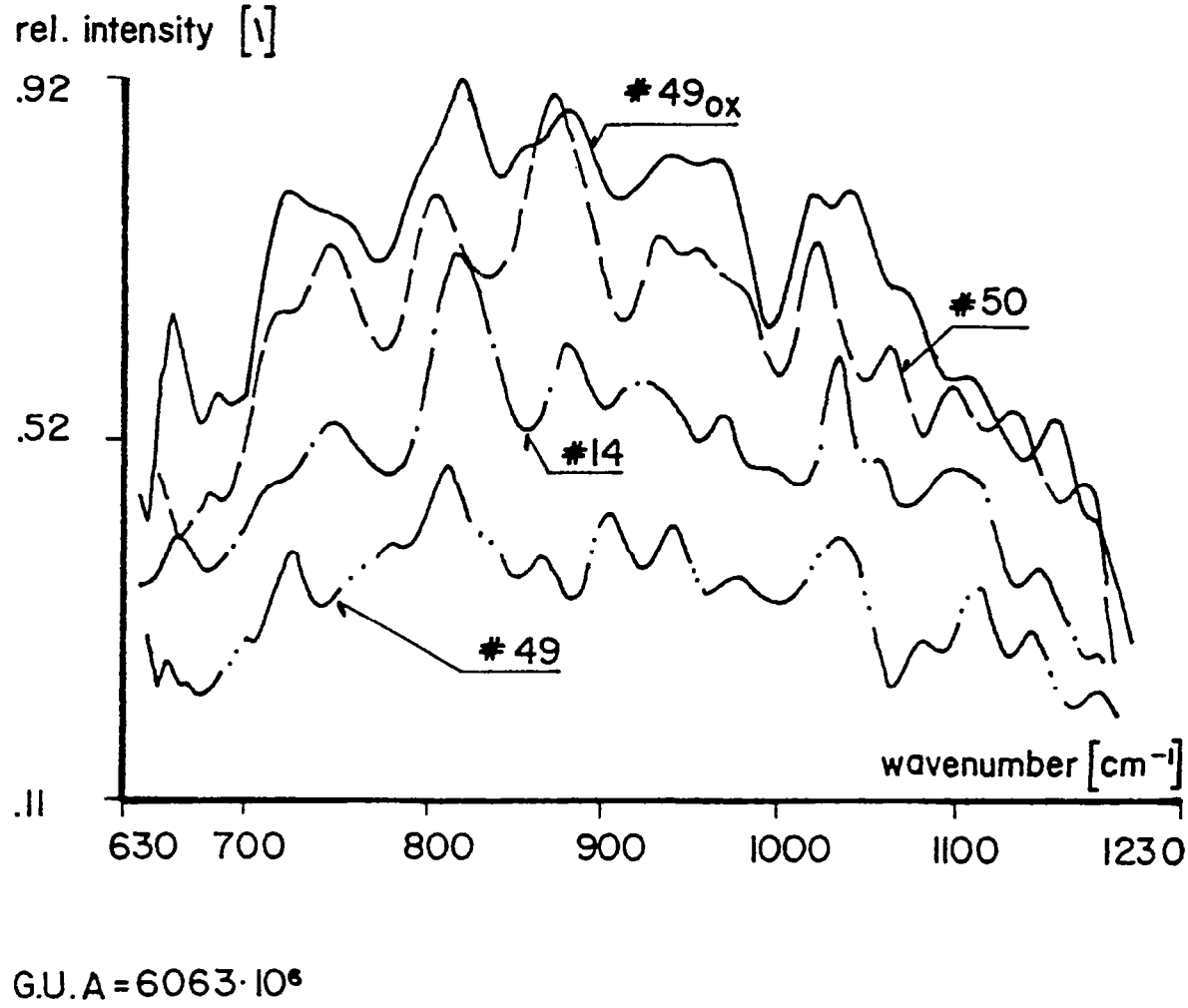

Figure 5.17 Comparison of Mode 1 spectra of the samples #14, #49, #50 with #49 after accelerated oxidation

and the 1010/1035 cm^{-1} doublet is made up of the 1010 cm^{-1} band of #50 and the 1035 cm^{-1} band of #49, etc. Now the bands grown in #49 after oxidation are also the prominent features of #14, the specimen allowed to sit in air for more than a year. Therefore, the tentative conclusion seems to be that rapid oxidation and sitting in air produces similar changes, but the latter produced the greater change.

PART 6

CONCLUSION

6.1 Lubricants in an EHD Contact

Reasons for studying the effect of TCE addition were these: (i) organic chlorides are frequent contaminants of lubricants and (ii) chlorides are highly adsorbed, even chemisorbed, on metal surfaces. Since TiN is non-metallic and very inert, TCE addition looked like a good way to study the effect of surface adsorption.

Let us take another look at Table 5.1. According to Hinterman and Boving [4], the thermal conductivity of TiN at 911°K is 0.088 watt/cm•K and at 1368°K it is 0.183 watt/cm•K. At both of these temperatures, the value of 440 C is expected to be at least two-to three-times higher and it is reasonable to assume that a similar ratio would be obtained at our--much lower--experimental temperatures. This would explain the higher T_B's when TCE is present: less heat is conducted away by the ball surface.

Higher T_B's would imply effectively lower viscosities, thinner EHD films, higher shear rates and therefore higher temperatures T_D at the diamond window which, in turn, imply higher tractions than those obtained with uncoated steel balls. Actually, however, tractions and diamond window temperatures T_D were lower (Table 5.1 and Figure 5.1) with the TiN-coated balls. Indeed, no scuffing occurred with the TiN-coated balls. Furthermore, as Figure 5.1 also showed, the effects of TCE on traction were much smaller for the TiN-coated balls than for the steel balls. While TCE always reducted traction with the steel balls, it reduced it slightly at low speed and increased it slightly at high speeds with the TiN-coated balls.

These results can be explained only by both a bulk and a surface effect ascribable to TCE. The model of Figure 6.1 is consistent with these observations. Additive materials accumulate in the inlet region of the Hertzian contact as another phase is formed under the positive pressure gradient. The flow lines have been shown even to reverse direction at the inlet. The conditions in the inlet region determine the film thickness and other properties of the following Hertzian contact region. An appreciable number of additive "globules" travel through the region in a two-phase flow (bulk effect). This model is consistent with Winer's view of traction in terms of limiting strength of the lubricant, considered as a glass in the Hertzian region. The pressure of the globules weakens this strength, especially when the material there has become glassy. The idea is similar to the resulting weakening of steel by substantial inclusions of undissolved particles. Hence, the friction, or traction, of a fluid can be substantially reduced by small amounts of impurities or additives and the effect can be independent of the nature of the surfaces. The present results comparing the TiN-coated balls with the steel balls show definite evidence of a strong surface effect with the steel balls for 5P4E with and without TCE. For only by assuming the existence of such layer can the higher temperatures generated be accounted for, the higher ΔT's of Table 5.2, with the uncoated steel balls than with the coated balls in spite of the formers' higher thermal conductivity: the effective shear rates are higher since the gap through which the lubricant is flowing is reduced by the adsorbed layers. Without TCE the adsorbed layers are 5P4E itself, with TCE, some of the

adsorbed 5P4E is replaced by TCE. This replacement is expected to produce a thinner boundary layer and therefore a thicker film of flowing lubricant and a lower film temperature and traction. The latter effect is shown dramatically in Figure 5.1 when the speed at which scuffing occurred was reduced by TCE by almost 50%. The somewhat higher traction caused by TCE at high speeds for both balls, though mostly for the coated ball, would seem to be primarily a bulk effect.

In our previous work, high traction was associated with high temperature rise in the gap and a comparison of the data of Table 5.2 with those of Figure 5.1 show that this parallelism is true for the present system as well. Clearly the temperature rise, ΔT, must be compared, not the initial temperature T_B. Molecular alignment, as indicated by the extent of polarization, is inversely related to temperature rise and traction. Thus, the alignment is greater when the coated ball is substituted for the uncoated ball and the diluted 5P4E for the undiluted, and these changes also decrease traction.

There seems to be little doubt that the molecular alignment, evidenced by the degree of polarization, is largely caused by the shear rate. Thus we are dealing with flow alignment or streaming dichroism. Table 5.3 shows the relationship clearly and Figures 5.6 and 5.7 show it as well. The difference in the sequence of increasing P with and without TCE in Table 5.3 is likely to be the bulk effect or two-phase flow in the presence of TCE. Since TCE comes out of solution at high pressure causing an effectively higher shear rate, the difference occurs at the higher Hertzian pressure. The degree of alignment at 1.2 ms^{-1} and 0.6 GPa is higher in the presence of TCE than in its

absence. The degree of alignment of the 5P4E molecules must be determined at the inlet; the more aligned the molecules at the inlet, the faster the flow throught the gap. Therefore, our spectrometer, which looks only at the gap sees a higher degree of flow alignment with the coated balls where the inlet temperatures are higher and therefore the viscosities lower. This work is believed to be the first EHD investigation where only the boundary surface was changed.

6.2 Aircraft Fuel Line Deposits

Fuels 1 and 2 (Figures 5.10 and 5.11) were of rather similar composition, but Fuel 3 was somewhat more aromatic. The conditions of deposit formation were not under our control. Not surprisingly, therefore, the deposit spectra (Mode 1) of the first two fuels resembled each other much more than either of them resembled the third deposit spectrum.

Let us consider the first two deposit spectra (Figures 5.10 and 5.11). The spectrum of Figure 5.10 has much higher contrast than that of Figure 5.11. The 780 cm^{-1} band is particular outstanding in Figure 5.10; the 745 cm^{-1} band is missing in Figure 5.10, but present in Figure 5.11. Examination of the Mode 2 spectra of Figure 5.10 does however, show an intense band at 745 cm^{-1} for the +30° phase angle. In fact, every band present in either spectrum is present in the other, though not necessarily in the Mode 1 spectrum or at the same phase angle in the Mode 2 spectra. A cursory examination of the two series of Mode 2 spectra will also show that most of the Fuel 1 spectra have greater spectral contrast (sharper bands) in the 630 - 900 cm^{-1} spectral region

than in the 1000 - 1230 cm^{-1} region, while the opposite is true for the Fuel 2 spectra. In either case, the sharpest bands are found in the $\pm$ 30° phase spectra, i.e. spectra in which the polarizer was displaced 30° from an arbitrary reference direction. It should also be recalled that Mode 2 spectral bands can point up or down (like absorption bands), since Mode 2 spectra are differences between two spectra.

The spectra of Fuel 3 are more different, as mentioned (Fig. 5.12). For example, the lowest frequency band in the Mode 1 spectrum is easily recognized as a doublet, and, indeed, the corresponding -30° phase angle Mode 2 spectrum has a sharp peak at 700 cm^{-1} That same Mode 2 spectrum has other outstandingly sharp bands at 780, 1020, 1100 and 1140 cm^{-1}.

The analysis of the aircraft fuel line deposits has shown: (i) a definite relationship between fuel composition and deposit composition (ii) orientation of deposits on their support and (iii) detection of weak bands by comparing spectral data acquired in different modes. It would seem that the band displacements of #50 with respect to #49 are newly grown bands, otherwise #49 oxidized would have single and not what appears to be clearly doublet bands. What are they due to? They are not caused by oxygen linkages, for the frequency region is wrong. Furthermore, if chemistry were primarily involved, one or more new bands would show rather than a number of bands getting satellites. Now it so happens that the outstanding characteristics of the 700 - 1200 cm^{-1} region are usually C-H deformations, fundamentals and overtones, which depend highly on crystallinity. For example, the CH_2-rocking fundamental occurs at $\sim$720 cm^{-1} in amorphous polyethylene, but

as a doublet 720/730 cm^{-1} in crystalline polyethylene. "Crystallinity" bands in polymers are at higher frequencies than "amorphous" bands. The reason for the cyrstallinity bands can be two polymer chains per unit cell, giving rise to interactions, or different effective chainlengths, because only the amorphous chaines can "curl" up.

One can speculate that higher temperatures or reheating a deposit in air change part of the deposit from the more crystalline to the more amorphous state. Greater adhesion of the deposit to the metal surface would be expected as a result. In other words, the changes on accelerated oxidation are caused by structural changes in the deposit.

6.3 Recommendations

The results of the analysis of aircraft fuel line deposits present just the beginning of a new series of experiments. With a set of systematically produced steel strips the structural changes should be confirmed.

The chemical analysis of the rather complex deposits is at the present very time-consuming. However further steps in data evaluation by computer can be taken. The spectra as plotted by the computer have to be transformed into the same format (bar diagram) as the data published in [21] for the identification of the bands. This step is not trivial at all since it envolves the recognition of bands by comparing the data of the same sample recorded in different modes. Computer graphics methods would allow the fast comparison of any two spectra, the identification of the frequency of a particular band and the generation of the bar diagram.

A recently published book [22] shows how to deconvolute absorption spectra. The increase in resolution gained by such a method would allow an easier unscrambling of complex spectra.

Indepth studies of the orientation of material includes the calculation of the intensity distribution function by deconvolution of relative band intensity as a function of phase angle with the polarizer line shape function. Based on these results molecular orientation can be determined.

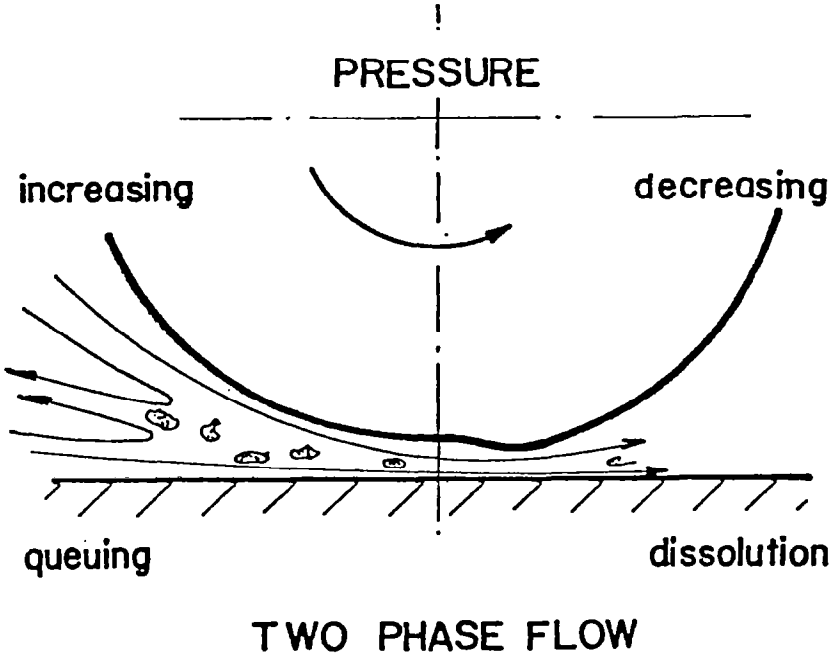

Figure 6.1 Model to explain the influence of trichloroethane (TCE) additive on flow dichrosim

PART 7

LITERATURE CITED

1. Bell, J.R., Introductory Fourier Transform Spectroscopy. Academic Press, Inc., New York, 1972.

2. King, V.W., "Emission Spectra from EHD Contacts." Dissertation R.P.I., Troy, N.Y., 1981.

3. Choi, F.H., "Ball/Plate Bearing Contact for Measuring Lubricant Film Thickness and Traction under Severe Operating Conditions," Master Thesis, R.P.I., Troy, N.Y., 1981.

4. Hintermann, H.E., Boving H. "Wearresistant Thin Layers." Die Technik, No. 7, 387-398, 1978 (in German).

5. Wilson, E.B., Molecular Vibrations. McGraw-Hill, New York, 1955.

6. Hudson, R.D., Infrared System Engineering. Wiley & Sons, New York, 1966.

7. Dowson, D. and Higginson, G.R., Elasto-Hydrodynamic Lubrication. Pergamon Press, 1977.

8. Goldstein, H., Classical Mechanics, Addison-Wesley Press, Cambridge, MA, 1956.

9. Eirich, F.R. (ed.), Rheology Vol. 1. Academic Press, Inc. p. 615, 1968.

10. Kuhn, W. and Kuhn, H., "Meaning of the limited degree of rotation for the viscosity and the flow birefringence of solutions of solutions of string-moleucles," Helv. Chim. Acta 28, 1533, 1945.

11. Lauer, J.L., Keller, L.E., Choi, F.H., and King, V.W., "Alignment of Fluid Molecules in an EHD Contact," ASLE Preprint No. 81-LC-5C-1, presented at the ASLE/ASME Lubrication Conference in New Orleans, LA, October 5-7, 1981.

12. Lauer, J.L. and Keller, L.E., "Analysis of Infrared Emission from Thin Absorbates," SPIE Vol. 289-1981, International Conference on Fourier Transform Spectroscopy, p. 87-93, 1981.

13. Lauer, J.L. and Keller, L.E., "Analysis of Aircraft Fuel Line Deposits by Polarization Infrared Fourier Emission Microscpectrophotometry," to be published in Surface Science.

14. Lauer, J.L. and Peterkin, M.E., "Analysis of Infrared Spectra of Fluid Films in Simulated EHD Contacts," ASME, Journal of Lubrication Technology, Vol 97, 145-150, 1975.

15. Lauer, J.L. and Peterkin, M.E., "Infrared Emission Spectra of Elastohydrodynamic Contacts," Trans. ASME Journal of Lubrication Technology, Vol. 98, 230-235, 1976.

16. Low, M.J.D. and Coleman, I., "The Measurement of Infrared Emission Spectra Using Multiple Scan Interferometry," Spectrochimica Acta, Vol 22, 369-376, 1966.

17. Alsaad, M., Bair, S., Sanborn, D.M., and Winer, W.D., "Glass Transitions in Lubricants: Its Relation to Elasto-Hydrodynamic Lubrication (EHD)." Trans. ASME, Journal of Lubrication Technology, Vol. 100, 404-417, 1978.

18. Okabe, H. and Kanno, T., "Behavior of Polar Compounds in Lubricating Oil Films," Trans. ASLE, Vol. 24, 459-466, 1981.

19. Rounds, F.G., "Effect of Aromatic Hydrocarbons on Friction and Surface Coating Formation with Three Additives." Trans. ASLE, Vol. 16, 141-149, 1973.

20. Griffiths, P.R., "Infrared Emission Spectroscopy. I. Basic Considerations," Applied Spectroscopy, Vol. 26, 1, 73-76, 1972.

21. Socrates, G. Infrared Characteristic Group Frequencies. Wiley & Sons, New York, 1980.

22. Blass, W.E. and Halsey, G.W., Deconvolution of Absorption Spectra, Academic Press, 1981.

1. Report No.	2. Government Accession No.	3. Recipient's Catalog No.
NASA CR-3658		

4. Title and Subtitle	5. Report Date
DETERMINATION OF PHYSICAL AND CHEMICAL STATES OF LUBRICANTS IN CONCENTRATED CONTACTS - PART 3	January 1983
	6. Performing Organization Code
7. Author(s)	8. Performing Organization Report No.
James L. Lauer and Leonhard Keller	None
	10. Work Unit No.
9. Performing Organization Name and Address	
Rensselaer Polytechnic Institute Dept. of Mech. Engineering, Aeronautical Engineering & Mechanics Troy, New York 12181	11. Contract or Grant No. NSG-3170
	13. Type of Report and Period Covered
12. Sponsoring Agency Name and Address	Contractor Report
National Aeronautics and Space Administration Washington, D. C. 20546	14. Sponsoring Agency Code 506-53-12 (E-1393)

15. Supplementary Notes

Final report. William R. Jones, Jr., Structures and Mechanical Technologies Division, NASA Lewis Research Center, Cleveland, Ohio 44135.

16. Abstract

Solid and liquid thin films have been analyzed by infrared emission Fourier microspectrophotometry. The apparatus used is a commercial absorption instrument modified to an emission instrument, comprising a rotating polarizing device, a miniature blackbody temperature reference adjustable in temperature and radiant flux and a microscope lens with a high numerical aperture in the entrance system for increased sensitivity and resolution. Studies of lubricant behavior in a simulated ball bearing showed the alignment of the fluid molecules in the Hertzian area. Polyphenyl ether plus 1% 1,1,2-trichloroethane (TCE) required lower shear rates for the same degree of alignment than without TCE. The experiment was run with 440 C stainless steel balls coated with TiN, a chemically inert material. In both cases, the alignment was strongly influenced by the presence of TCE. The results showed (i) the dependence of alignment of fluid molecules on flow and not on adsorption at metallic surfaces, (ii) phase separation between lubricant and additive under high pressure which results in two-phase flow and (iii) reduction in traction of torque-transmitting (traction) fluids. Measurements of phase separation, by differential thermal analysis and in a high pressure cell, and traction measurements confirmed the spectral results. With the same instrument solid deposits on aircraft fuel lines were studied. These materials were deposited in a preferred direction. Despite the strong background radiation and the presence of a multitude of compounds, the spectral contrast was sufficient to establish a relationship between fuel and deposit composition. Comparison of a one year old sample with a sample exposed to accelerated oxidation showed little difference. The originally crystalline structure became amorphous and therefore more tacky. This result shows the reactivity of initial deposits and the need for storing them with care.

17. Key Words (Suggested by Author(s))	18. Distribution Statement
Fourier transform spectroscopy Elastohydrodynamics	Unclassified - unlimited STAR Category 27

19. Security Classif. (of this report)	20. Security Classif. (of this page)	21. No. of Pages	22. Price*
Unclassified	Unclassified	109	A06

* For sale by the National Technical Information Service, Springfield, Virginia 22161

NASA-Langley, 1983